

# Decoding the phases of early and late time reheating through imprints on primordial gravitational waves

Md Riajul Haque,<sup>1,\*</sup> Debaprasad Maity,<sup>1,†</sup> Tanmoy Paul,<sup>2,3,‡</sup> and L. Sriramkumar<sup>4,§</sup>

<sup>1</sup>*Department of Physics, Indian Institute of Technology, Guwahati 781039, India*

<sup>2</sup>*Department of Physics, Chandernagore College, Hooghly 712136, India*

<sup>3</sup>*International Laboratory for Theoretical Cosmology, TUSUR, 634050 Tomsk, Russia*

<sup>4</sup>*Department of Physics, Indian Institute of Technology Madras, Chennai 600036, India*

Primordial gravitational waves (GWs) carry the imprints of the dynamics of the universe during its earliest stages. With a variety of GW detectors being proposed to operate over a wide range of frequencies, there is great expectation that observations of primordial GWs can provide us with an unprecedented window to the physics operating during inflation and reheating. In this work, we closely examine the effects of the regime of reheating on the spectrum of primordial GWs observed today. We consider a scenario wherein the phase of reheating is described by an averaged equation of state (EoS) parameter with an abrupt transition to radiation domination as well as a scenario wherein there is a gradual change in the effective EoS parameter to that of radiation due to the perturbative decay of the inflaton. We show that the perturbative decay of the inflaton leads to oscillations in the spectrum of GWs, which, if observed, can possibly help us decipher finer aspects of the reheating mechanism. We also examine the effects of a secondary phase of reheating arising due to a brief epoch driven possibly by an exotic, non-canonical, scalar field. Interestingly, we find that, for suitable values of the EoS parameter governing the secondary phase of reheating, the GWs can be of the strength as suggested by the recent NANOGrav observations. We conclude with a discussion of the wider implications of our analysis.

## I. INTRODUCTION

The inflationary scenario offers the most attractive mechanism for the generation of the primordial perturbations (for the original discussions, see Refs. [1–4]; for reviews, see, for example, Refs. [5–14]). The existence of primordial gravitational waves (GWs) is one of the profound predictions of inflationary dynamics (for the initial discussions, see, for example, Refs. [15, 16]; for recent reviews on the generation of primary and secondary GWs, see, for instance, Refs. [17, 18]). If the primordial GWs or their imprints are detected, it will not only prove the quantum origin of the perturbations, it can also, in principle, provide us with insights into the fundamental nature of gravitation. The primordial GWs provide a unique window to probe the dynamics of our universe during its very early stages, which seems difficult to observe by any other known means. However, the extremely weak nature of the gravitational force makes the detection of GWs rather challenging. Decades of effort towards detecting GWs have finally achieved success only in the last few years with the observations of GWs from merging binary black holes and neutron stars by LIGO [19–30]. These observations have led to a surge of experimental proposals across the globe to observe GWs over a wide range of frequencies. The proposed GW observatories include advanced LIGO (10–10<sup>3</sup> Hz) [31], ET (1–10<sup>4</sup> Hz) [32, 33], BBO (10<sup>–3</sup>–10 Hz) [34–36], DECIGO (10<sup>–3</sup>–1 Hz) [37–40], eLISA (10<sup>–5</sup>–1 Hz) [41–43], and SKA (10<sup>–9</sup>–10<sup>–6</sup> Hz) [44].

Apart from various astrophysical mechanisms that can generate GWs, as we mentioned, inflation provides an exclusive mechanism to produce GWs of quantum mechanical origin (for discussions on the generation of primary and secondary GWs, see, for instance, Refs. [45–58] and references therein). The tensor perturbations generated from the quantum vacuum are amplified during inflation, which subsequently evolve through the various phases of the universe until they reach the GW detectors today. Therefore, the spectrum of primordial GWs today is a convolution of their origin as well as dynamics. On the one hand, they contain the signatures of the mechanism that generates them, viz. the specific model that drives inflation as well as the initial conditions from which the perturbations emerge. On the other, they also carry the imprints of the dynamics of the subsequent cosmological phases as the GWs propagate through them. As is well known, immediately after inflation, the universe is expected to be reheated through the decay of the inflaton into radiation, which eventually leads to the epoch of radiation domination. In this work, we shall examine the evolution of primordial GWs with special emphasis on the effects due to the epoch of reheating. Specifically, our aim is to decode the mechanism of reheating from the spectrum of GWs today.

---

\* E-mail: [riaju176121018@iitg.ac.in](mailto:riaju176121018@iitg.ac.in)

† E-mail: [debu@iitg.ac.in](mailto:debu@iitg.ac.in)

‡ E-mail: [pul.tnmy9@gmail.com](mailto:pul.tnmy9@gmail.com)

§ E-mail: [sriram@physics.iitm.ac.in](mailto:sriram@physics.iitm.ac.in)

Over the years, major cosmological observations have considerably improved the theoretical understanding of the various epochs of our universe [59–61]. However, due to the lack of direct observational signatures, the phase of reheating remains poorly understood. The effects of reheating on the dynamics of GWs have already been examined in the standard cosmological scenario (see, for instance, Refs. [62–69]) as well as in certain non-standard scenarios (see, for example, Refs. [70–80]). Moreover, the imprints of specific microscopic physical effects on the spectrum of GWs — such as decoupling neutrinos [81, 82] or the variation in the number of relativistic degrees of freedom in the early universe [83–85] — have also been explored. In this work, we shall study the effects of reheating on the spectrum of primordial GWs over a wide range of scales and illustrate the manner in which the spectrum captures specific aspects of the different phases. We shall consider two of the simplest reheating mechanisms. We shall first consider a scenario wherein the reheating phase is described by an averaged equation of state (EoS) parameter, with reheating ending instantaneously [86–88]. We shall then consider a scenario wherein there is a gradual change in the EoS parameter from its initial value during the phase of coherent oscillations to its eventual value during radiation domination achieved through the perturbative decay of the inflaton [89–93]. We shall explicitly illustrate the effects of the reheating dynamics on the spectrum of GWs. It seems worthwhile to highlight here that the following aspects of the reheating dynamics can, in principle, be decoded from the spectrum of primordial GWs: (i) the shape of the inflaton potential near its minimum which is responsible for the end of inflation and the dynamics during reheating, (ii) the decay width of the inflaton, which governs the entire process of reheating and therefore determines the reheating temperature, and (iii) the thermalization time scale over which the EoS parameter during the period of coherent oscillations of the inflaton say,  $w_\phi$ , is modified to the EoS parameter corresponding to radiation. Further, it is expected that determining the inflaton decay width and the thermalization time scale would permit us not only to arrive at the form of the coupling between the inflaton and radiation, but also help us understand the nature of the coupling amongst all the relativistic degrees of freedom. We shall briefly discuss these possibilities in this work, and we shall return to examine the issue in greater detail in a future effort.

Finally, we shall also consider the implications of our analysis on the recent observations involving the pulsar-timing data by the North American Nanohertz Observatory for Gravitational Waves (NANOGrav), which has been attributed to stochastic GWs [94, 95]. A variety of mechanisms that can possibly occur in the early universe have been explored in the literature to explain this interesting observation [58, 96–109]. We find that introducing a secondary phase of reheating — apart from the original, inflaton driven, primary reheating phase — can account for the NANOGrav observations. We introduce an exotic, non-canonical scalar field to drive such a phase and show that a suitable EoS for the non-canonical field can lead to primordial GWs of strength as observed by NANOGrav.

This paper is structured as follows. In Sec. II, we shall briefly sketch the arguments leading to the standard scale-invariant spectrum of GWs generated in de Sitter inflation. We shall also discuss the typical inflationary model that we shall have in mind when we later discuss the effects due to reheating. Moreover, we shall introduce the dimensionless density parameter  $\Omega_{\text{GW}}$  characterizing the spectrum of GWs. In Sec. III, we shall discuss the evolution of the tensor perturbations during the epoch of reheating. We shall first consider the scenario wherein the epoch of reheating is described by an averaged EoS parameter associated with the inflaton. Such a description allows us to arrive at analytic solutions for the tensor perturbations during the epoch. We shall also consider the scenario of perturbative reheating wherein we take into account the continuous decay of the inflaton into radiation. As it proves to be involved in constructing analytical solutions for the background as well as the tensor perturbations in such a case, we shall resort to numerics. In Sec. IV, we shall briefly discuss the evolution of the tensor perturbations during the epoch of radiation domination and arrive at the spectrum of GWs today by comparing the behavior of the the energy density of GWs in the sub-Hubble domain with that of radiation. In Secs. V and VI, we shall evaluate the dimensionless energy density of GWs today that arise in the two types of reheating scenarios mentioned above. We shall focus on the spectrum of primordial GWs over wave numbers (or, equivalently, frequencies) that correspond to small scales which reenter the Hubble radius either during the epochs of reheating or radiation domination. In Sec. VII, we shall numerically evaluate the inflationary tensor power spectrum and discuss the behavior of the spectrum of GWs today close to the scale that leaves the Hubble radius at the end of inflation. In Sec. VIII, we shall outline the manner in which we should be able to decode various information concerning the epochs of inflation and reheating from the observations of the anisotropies in the cosmic microwave background (CMB) and the spectrum of GWs today. In Sec. IX, we shall evaluate the spectrum of GWs in a scenario involving late time production of entropy and discuss the implications for the recent observations by NANOGrav. Lastly, in Sec. X, we shall conclude with a summary of the main results.

Before we proceed further, a few clarifications concerning the conventions and notations that we shall adopt are in order. We shall work with natural units such that  $\hbar = c = 1$ , and set the reduced Planck mass to be  $M_{\text{Pl}} = (8\pi G)^{-1/2}$ . We shall adopt the signature of the metric to be  $(-, +, +, +)$ . Note that Latin indices shall represent the spatial coordinates, except for  $k$ , which shall be reserved for denoting the wavenumber of the tensor perturbations, i.e. GWs. We shall assume the background to be the spatially flat Friedmann-Lemaître-Robertson-Walker (FLRW) line element described by the scale factor  $a$  and the Hubble parameter  $H$ . Also, an overprime shall denote differentiation with

respect to the conformal time  $\eta$ . We should mention that the frequency, say,  $f$ , is related to the wave number  $k$  of the tensor perturbations through the relation

$$f = \frac{k}{2\pi} = 1.55 \times 10^{-15} \left( \frac{k}{1 \text{ Mpc}^{-1}} \right) \text{ Hz} \quad (1)$$

and, as convenient, we shall refer to the spectrum of GWs either in terms of wave numbers or frequencies.

## II. SPECTRUM OF GWS GENERATED DURING INFLATION

In this section, we shall briefly recall the equation governing the tensor perturbations and arrive at the spectrum of GWs generated in de Sitter inflation. We shall also introduce the dimensionless energy density of GWs, which is the primary observational quantity of interest in this work.

### A. Generation of GWs during inflation

Let  $h_{ij}$  denote the tensor perturbations characterizing the GWs in a FLRW universe. When these tensor perturbations are taken into account, the line-element describing the spatially flat, FLRW universe can be expressed as [110]

$$ds^2 = a^2(\eta) \left\{ -d\eta^2 + [\delta_{ij} + h_{ij}(\eta, \mathbf{x})] dx^i dx^j \right\}. \quad (2)$$

Since the tensor perturbations are transverse and traceless, they satisfy the conditions  $\partial^i h_{ij} = 0$  and  $h_i^i = 0$ . We shall assume that no anisotropic stresses are present. In such a case, the first order Einstein's equations then lead to the following equation of motion for the tensor perturbations  $h_{ij}$ :

$$h_{ij}'' + 2 \frac{a'}{a} h_{ij}' - \nabla^2 h_{ij} = 0. \quad (3)$$

On quantization, the tensor perturbations can be decomposed in terms of the Fourier modes  $h_k$  as follows [5-14]:

$$\begin{aligned} \hat{h}_{ij}(\eta, \mathbf{x}) &= \int \frac{d^3 \mathbf{k}}{(2\pi)^{3/2}} \hat{h}_{ij}^{\mathbf{k}}(\eta) e^{i \mathbf{k} \cdot \mathbf{x}} \\ &= \sum_{\lambda=+, \times} \int \frac{d^3 \mathbf{k}}{(2\pi)^{3/2}} \left[ \hat{a}_{\mathbf{k}}^\lambda \varepsilon_{ij}^\lambda(\mathbf{k}) h_k(\eta) e^{i \mathbf{k} \cdot \mathbf{x}} + \hat{a}_{\mathbf{k}}^{\lambda\dagger} \varepsilon_{ij}^{\lambda*}(\mathbf{k}) h_k^*(\eta) e^{-i \mathbf{k} \cdot \mathbf{x}} \right], \end{aligned} \quad (4)$$

where the quantity  $\varepsilon_{ij}^\lambda(\mathbf{k})$  represents the polarization tensor, with the index  $\lambda$  denoting the polarization  $+$  or  $\times$  of the GWs. The polarization tensor obeys the relations  $\delta^{ij} \varepsilon_{ij}^\lambda(\mathbf{k}) = k^i \varepsilon_{ij}^\lambda(\mathbf{k}) = 0$ , and we shall work with the normalization such that  $\varepsilon^{ij \lambda}(\mathbf{k}) \varepsilon_{ij}^{\lambda'*}(\mathbf{k}) = 2 \delta^{\lambda\lambda'}$ . In the above decomposition, the operators ( $\hat{a}_{\mathbf{k}}^\lambda, \hat{a}_{\mathbf{k}}^{\lambda\dagger}$ ) denote the annihilation and creation operators corresponding to the tensor modes associated with the wave vector  $\mathbf{k}$ . They obey the following commutation relations:  $[\hat{a}_{\mathbf{k}}^\lambda, \hat{a}_{\mathbf{k}'}^{\lambda'}] = [\hat{a}_{\mathbf{k}}^{\lambda\dagger}, \hat{a}_{\mathbf{k}'}^{\lambda'\dagger}] = 0$  and  $[\hat{a}_{\mathbf{k}}^\lambda, \hat{a}_{\mathbf{k}'}^{\lambda'\dagger}] = \delta^{(3)}(\mathbf{k} - \mathbf{k}') \delta^{\lambda\lambda'}$ . In the absence of sources with anisotropic stresses, the Fourier mode  $h_k$  satisfies the differential equation

$$h_k'' + 2 \frac{a'}{a} h_k' + k^2 h_k = 0. \quad (5)$$

The tensor power spectrum  $\mathcal{P}_T(k)$  is defined through the relation

$$\langle 0 | \hat{h}_{\mathbf{k}}^{ij}(\eta) \hat{h}_{\mathbf{k}'}^{\mathbf{k}'}(\eta) | 0 \rangle = \frac{(2\pi)^2}{2k^3} \mathcal{P}_T(k) \delta^{(3)}(\mathbf{k} + \mathbf{k}'), \quad (6)$$

where the vacuum state  $|0\rangle$  is defined as  $\hat{a}_{\mathbf{k}}^\lambda |0\rangle = 0$  for all  $\mathbf{k}$  and  $\lambda$ . On utilizing the above decomposition in terms of the Fourier modes, we obtain that

$$\mathcal{P}_T(k) = 4 \frac{k^3}{2\pi^2} |h_k|^2, \quad (7)$$

and it is often assumed that the spectrum is evaluated on super-Hubble scales during inflation.

Motivated by form of the second order action governing the tensor perturbation  $h_{ij}$ , the Fourier mode  $h_k$  is usually written in terms of the Mukhanov-Sasaki variable  $u_k$  as  $h_k = (\sqrt{2}/M_{\text{Pl}})(u_k/a)$ . The Mukhanov-Sasaki variable  $u_k$  satisfies the differential equation [5–14]

$$u_k'' + \left(k^2 - \frac{a''}{a}\right) u_k = 0. \quad (8)$$

We shall focus on the simple case of slow roll inflation and work in the de Sitter approximation wherein the scale factor is given by  $a(\eta) = (1 - H_1 \eta)^{-1}$ , with  $H_1$  denoting the constant Hubble scale during inflation. In such a case,  $a''/a = 2H_1^2/(1 - H_1 \eta)^2$ , and the solution to Eq. (8) corresponding to the Bunch-Davies initial condition is given by

$$u_k(\eta) = \frac{1}{\sqrt{2}k} \left[ 1 + \frac{i H_1 a(\eta)}{k} \right] e^{-ik\eta}. \quad (9)$$

Or, equivalently, we can write that

$$h_k(\eta) = h_k(a) = \frac{\sqrt{2}}{M_{\text{Pl}}} \frac{i H_1}{\sqrt{2}k^3} \left[ 1 - \frac{ik}{H_1 a(\eta)} \right] e^{-ik/H_1} e^{ik/[H_1 a(\eta)]} \quad (10)$$

with  $a(\eta)$  being given by the de Sitter form mentioned above. Let us assume that inflation ends at the conformal time  $\eta_f$  such that  $0 < \eta_f < H_1^{-1}$ , and let  $a_f = a(\eta_f)$ . Under these conditions, upon using the above solution, the tensor power spectrum at  $a_f$  can be obtained to be

$$\mathcal{P}_{\text{T}}(k) = \frac{2H_1^2}{\pi^2 M_{\text{Pl}}^2} \left( 1 + \frac{k^2}{k_f^2} \right), \quad (11)$$

where  $k_f = a_f H_1$  is the mode that leaves the Hubble radius at the end of inflation. For  $k \ll k_f$ , the above spectrum reduces to

$$\mathcal{P}_{\text{T}}(k) \simeq \frac{2H_1^2}{\pi^2 M_{\text{Pl}}^2}, \quad (12)$$

which is the well known scale invariant spectrum often discussed in the context of de Sitter inflation [5–14]. Actually, in slow roll inflation, the tensor power spectrum will contain a small spectral tilt, which we shall choose to ignore in our discussion. We should emphasize the point that the above scale invariant spectrum is valid only for  $k \ll k_f$  since the de Sitter form for the scale factor would not hold true close to the end of inflation. Therefore, in our discussion below, we shall mostly restrict ourselves to wave numbers such that  $k < 10^{-2} k_f$ . In Sec. VII, we shall evaluate tensor power spectrum numerically in the inflationary model of interest to arrive at the present day spectrum of GWs near  $k_f$ .

## B. A typical inflationary model of interest

In order to illustrate the results later, we shall focus on a specific inflationary model that permits slow roll inflation. We shall consider the so-called  $\alpha$ -attractor model, which unifies a large number of inflationary potentials (in this context, see Refs. [111, 112]). If  $\phi$  is the canonical scalar field driving inflation, the model is described by the potential  $V(\phi)$  of the form

$$V(\phi) = \Lambda^4 \left[ 1 - \exp \left( -\sqrt{\frac{2}{3\alpha}} \frac{\phi}{M_{\text{Pl}}} \right) \right]^{2n}, \quad (13)$$

where, as we shall soon discuss, the scale  $\Lambda$  can be determined using the constraints from the observations of the anisotropies in the CMB. It is worth pointing out here that, for  $n = 1$  and  $\alpha = 1$ , the above potential reduces to the Higgs-Starobinsky model [113, 114]. We should also mention that the potential (13) contains a plateau at suitably large values of the field, which is favored by the CMB data [59].

Let  $N_k$  denote the e-fold at which the wave number  $k$  leaves the Hubble radius, *when counted from the end of inflation*. For the potential (13), the quantity  $N_k$  can be easily determined in the slow roll approximation to be (see, for instance, Ref. [115])

$$N_k \simeq \frac{3\alpha}{4n} \left[ \exp \left( \sqrt{\frac{2}{3\alpha}} \frac{\phi_k}{M_{\text{Pl}}} \right) - \exp \left( \sqrt{\frac{2}{3\alpha}} \frac{\phi_f}{M_{\text{Pl}}} \right) - \sqrt{\frac{2}{3\alpha}} \left( \frac{\phi_k}{M_{\text{Pl}}} - \frac{\phi_f}{M_{\text{Pl}}} \right) \right], \quad (14)$$

where  $\phi_k$  and  $\phi_f$  denote the values of the field when the mode with wave number  $k$  crosses the Hubble radius and at the end of inflation, respectively. It is easy to show that  $\phi_f$  can be expressed in terms of the parameters  $\alpha$  and  $n$  as

$$\frac{\phi_f}{M_{\text{Pl}}} \simeq \sqrt{\frac{3\alpha}{2}} \ln \left( \frac{2n}{\sqrt{3\alpha}} + 1 \right). \quad (15)$$

As we mentioned, the parameter  $\Lambda$  can be determined by utilizing the constraints from the CMB. One finds that the parameter can be expressed in terms of the scalar amplitude  $\mathcal{A}_s$ , the scalar spectral index  $n_s$  and the tensor-to-scalar ratio  $r$  as follows:

$$\Lambda = M_{\text{Pl}} \left( \frac{3\pi^2 r \mathcal{A}_s}{2} \right)^{1/4} \left[ \frac{2n(1+2n) + \sqrt{4n^2 + 6\alpha(1+n)(1-n_s)}}{4n(1+n)} \right]^{n/2}. \quad (16)$$

Given the best-fit values for the inflationary parameters  $\mathcal{A}_s$  and  $n_s$  as well as the upper bound on  $r$  from Planck [59], evidently, using the above relation, we can choose a set of values for the parameters  $\Lambda$ ,  $\alpha$  and  $n$  describing the potential (13) that are compatible with the CMB data.

As we shall see, to evolve the background beyond inflation, we shall require the value of the energy density of the scalar field at the end of inflation, say,  $\rho_f$ . One finds that the quantity  $\rho_f$  can be expressed in terms of the corresponding value of the potential, say,  $V_f$ , as

$$\rho_f = \frac{3}{2} V_f. \quad (17)$$

It is useful to note here that the value of the potential (13) at the end of inflation is given by

$$V_f = V(\phi_f) = \Lambda^4 \left( \frac{2n}{2n + \sqrt{3\alpha}} \right)^{2n}. \quad (18)$$

We should mention that, hereafter, we shall set the parameter  $\alpha$  to be unity.

### C. The dimensionless energy density of GWs

Let us turn to now discuss the observable quantity of our interest, viz. the dimensionless energy density of GWs. We shall be interested in evaluating the quantity over the domain of wave numbers which reenter the Hubble radius during the epochs of reheating and radiation domination.

The energy density of GWs at any given time, say,  $\rho_{\text{GW}}(\eta)$ , is given by (see, for example, Refs. [63, 110])

$$\rho_{\text{GW}}(\eta) = \frac{M_{\text{Pl}}^2}{4a^2} \left( \frac{1}{2} \langle \hat{h}'_{ij}{}^2 \rangle + \frac{1}{2} \langle |\nabla \hat{h}_{ij}|^2 \rangle \right), \quad (19)$$

where the expectation values are to be evaluated in the initial Bunch-Davies vacuum imposed in the sub-Hubble regime during inflation. The energy density per logarithmic interval, say,  $\rho_{\text{GW}}(k, \eta)$ , is defined through the relation

$$\rho_{\text{GW}}(\eta) = \int_0^\infty d \ln k \rho_{\text{GW}}(k, \eta). \quad (20)$$

Upon using the mode decomposition (4) and the above expressions for  $\rho_{\text{GW}}(\eta)$ , we obtain the quantity  $\rho_{\text{GW}}(k, \eta)$  to be

$$\rho_{\text{GW}}(k, \eta) = \frac{M_{\text{Pl}}^2}{a^2} \frac{k^3}{2\pi^2} \left( \frac{1}{2} |h'_k(\eta)|^2 + \frac{k^2}{2} |h_k(\eta)|^2 \right). \quad (21)$$

The corresponding dimensionless energy density  $\Omega_{\text{GW}}(k, \eta)$  is defined as

$$\Omega_{\text{GW}}(k, \eta) = \frac{\rho_{\text{GW}}(k, \eta)}{\rho_c(\eta)} = \frac{\rho_{\text{GW}}(k, \eta)}{3H^2 M_{\text{Pl}}^2}, \quad (22)$$

where  $\rho_c = 3H^2 M_{\text{Pl}}^2$  is the critical density at time  $\eta$ .

The observable quantity of interest is the dimensionless energy density  $\Omega_{\text{GW}}(k, \eta)$  evaluated *today*, which we shall denote as  $\Omega_{\text{GW}}(k)$ . We shall often refer to  $\Omega_{\text{GW}}(k)$  or, equivalently,  $\Omega_{\text{GW}}(f)$  [recall that  $f$  is the frequency associated with the wave number  $k$ , cf. Eq. (1)], as the spectrum of GWs today. In the following sections, we shall evolve the tensor perturbations through the epochs of reheating and radiation domination. As we shall see, at late times during radiation domination, once all the wave numbers of interest are well inside the Hubble radius, the energy density of GWs behave in a manner similar to that of the energy density of radiation. We shall utilize this behavior to arrive at the spectrum of GWs today.

### III. EVOLUTION OF GWS DURING REHEATING

In order to follow the evolution of the tensor perturbations post inflation, it proves to be convenient to write (in this context, see, for instance, Ref. [63])

$$h_k(\eta) = h_k^{\text{P}} \chi_k(\eta), \quad (23)$$

where  $h_k^{\text{P}}$  denotes the primordial value evaluated at the end of inflation, and is given by [cf. Eq. (10)]

$$h_k^{\text{P}} = h_k(a_{\text{f}}) = \frac{\sqrt{2}}{M_{\text{Pl}}} \frac{i H_{\text{I}}}{\sqrt{2} k^3} \left(1 - \frac{i k}{k_{\text{f}}}\right) e^{-i k/H_{\text{I}}} e^{i k/k_{\text{f}}}. \quad (24)$$

The quantity  $\chi_k$  is often referred to as the tensor transfer function, which obeys same equation of motion as  $h_k$ , viz. Eq. (5). Clearly, the strength of the primordial GWs observed today will not only depend on the amplitude of the tensor perturbations generated during inflation, but also on their evolution during the subsequent epochs. In this section, we shall discuss the evolution of the transfer function  $\chi_k$  during the epoch of reheating. As we mentioned earlier, we shall consider two types of scenarios for reheating. We shall first consider the case wherein the period of reheating is described by the constant EoS parameter, say,  $w_\phi$ , often associated with the coherent oscillations of the scalar field around the minimum of the inflationary potential. We shall assume that the transition to radiation domination occurs instantaneously after a certain duration of time. In such a case, as we shall see, the transfer function  $\chi_k$  can be arrived at analytically. We shall then consider the scenario of perturbative reheating wherein there is a gradual transfer of energy from the inflaton to radiation. It seems difficult to treat such a situation analytically and, hence, we shall examine the problem numerically.

To follow the evolution of GWs in the post-inflationary regime, we shall choose to work with rescaled scale factor as the independent variable rather than the conformal time coordinate. If we define  $A = a/a_{\text{f}}$ , where  $a_{\text{f}} = a(\eta_{\text{f}})$  is the scale factor at the end of inflation, then we find that the equation governing the transfer function  $\chi_k$  is given by

$$\frac{d^2 \chi_k}{dA^2} + \left(\frac{4}{A} + \frac{1}{H} \frac{dH}{dA}\right) \frac{d\chi_k}{dA} + \frac{(k/k_{\text{f}})^2}{(H/H_{\text{I}})^2 A^4} \chi_k = 0, \quad (25)$$

where, recall that,  $k_{\text{f}} = a_{\text{f}} H_{\text{I}}$  denotes the wave number that leaves the Hubble radius at the end of inflation. Our aim now is to solve the above equation for the transfer function during the epoch of reheating. As is evident from the equation, the evolution of GWs is dictated by the behavior of the Hubble parameter. Therefore, if we can first determine the behavior of the Hubble parameter during reheating, we can solve the above equation to understand the evolution of transfer function  $\chi_k$  during the epoch. We shall also require the initial conditions for the transfer function  $\chi_k$  and its derivative  $d\chi_k/dA$  at the end of inflation, i.e. when  $a = a_{\text{f}}$  or, equivalently, when  $A = 1$ . Since we have introduced the transfer function through the relation (23), clearly,

$$\chi_k^{\text{I}}(A = 1) = 1. \quad (26)$$

Also, on using the solution (10) and the expression (24) for  $h_k^{\text{P}}$ , we find that

$$\frac{d\chi_k^{\text{I}}(A = 1)}{dA} = -\frac{(k/k_{\text{f}})^2}{1 - i(k/k_{\text{f}})} \simeq 0, \quad (27)$$

where the final equality is applicable when  $k \ll k_{\text{f}}$ . We shall make use of these initial conditions to determine the transfer function during the epoch of reheating.

In the following two sub-sections, we shall discuss the solutions in the two scenarios involving instantaneous and gradual transfer of energy from the inflaton to radiation.

#### A. Reheating described by an averaged EoS parameter

Let us first consider the scenario wherein the epoch of reheating is dominated by the dynamics of the scalar field as it oscillates at the bottom of an inflationary potential, such as the  $\alpha$ -attractor model (13) we had introduced earlier. In such a case, the evolution of the scalar field can be described by an averaged EoS parameter, say,  $w_\phi$  [86–88]. The conservation of energy implies that the energy density of the inflaton behaves as  $\rho_\phi \propto a^{-3(1+w_\phi)}$ , which, in turn, implies that the Hubble parameter behaves as  $H^2 = H_{\text{I}}^2 A^{-3(1+w_\phi)}$ . Note that,  $H = H_{\text{I}}$  when  $A = 1$ , as required. As a result, during such a phase, equation (25) governing the tensor transfer function reduces to the form

$$\frac{d^2 \chi_k}{dA^2} + (5 - 3w_\phi) \frac{1}{2A} \frac{d\chi_k}{dA} + \frac{(k/k_{\text{f}})^2}{A^{1-3w_\phi}} \chi_k = 0. \quad (28)$$



The general solution to this differential equation can be expressed as

$$\chi_k^{\text{RH}}(A) = A^{-\nu} \left[ C_k J_{-\nu/\gamma} \left( \frac{k}{\gamma k_f} A^\gamma \right) + D_k J_{\nu/\gamma} \left( \frac{k}{\gamma k_f} A^\gamma \right) \right], \quad (29)$$

where  $J_\alpha(z)$  denote Bessel functions of order  $\alpha$ , while the quantities  $\nu$  and  $\gamma$  are given by

$$\nu = \frac{3}{4}(1 - w_\phi), \quad \gamma = \frac{1}{2}(1 + 3w_\phi). \quad (30)$$

The coefficients  $C_k$  and  $D_k$  can be arrived at by using the conditions (26) and (27) for the transfer function  $\chi_k$  and its derivative  $d\chi_k/dA$  at end of inflation, i.e. when  $A = 1$ . We find that the coefficients  $C_k$  and  $D_k$  can be expressed as follows:

$$C_k = \frac{\pi k}{2\gamma k_f} \left[ \frac{1}{1 - i(k/k_f)} \right] \left[ \frac{k}{k_f} J_{\nu/\gamma} \left( \frac{k}{\gamma k_f} \right) - \left( 1 - \frac{ik}{k_f} \right) J_{(\nu/\gamma)+1} \left( \frac{k}{\gamma k_f} \right) \right] \csc \left( \frac{\pi\nu}{\gamma} \right), \quad (31a)$$

$$D_k = -\frac{\pi k}{2\gamma k_f} \left[ \frac{1}{1 - i(k/k_f)} \right] \left[ \frac{k}{k_f} J_{-\nu/\gamma} \left( \frac{k}{\gamma k_f} \right) + \left( 1 - \frac{ik}{k_f} \right) J_{-(\nu/\gamma)-1} \left( \frac{k}{\gamma k_f} \right) \right] \csc \left( \frac{\pi\nu}{\gamma} \right). \quad (31b)$$

We shall later make use of these coefficients and the solution (29) to eventually arrive at the spectrum of GWs today. It is useful to note here that the quantity  $d\chi_k^{\text{RH}}/dA$  is given by

$$\frac{d\chi_k^{\text{RH}}}{dA} = \frac{k}{k_f} A^{-1+\gamma-\nu} \left[ C_k J_{-(\nu/\gamma)-1} \left( \frac{k}{\gamma k_f} A^\gamma \right) - D_k J_{(\nu/\gamma)+1} \left( \frac{k}{\gamma k_f} A^\gamma \right) \right]. \quad (32)$$

We should mention here that the duration of the reheating phase characterized by the number of e-folds  $N_{\text{re}}$  and the reheating temperature  $T_{\text{re}}$  can be expressed in terms of the equation of state parameter  $w_\phi$  and the inflationary parameters as follows (in this context, see, for example, Refs. [87, 88]):

$$N_{\text{re}} = \frac{4}{(3w_\phi - 1)} \left[ N_* + \frac{1}{4} \ln \left( \frac{30}{\pi^2 g_{\text{r, re}}} \right) + \frac{1}{3} \ln \left( \frac{11 g_{\text{s, re}}}{43} \right) + \ln \left( \frac{k_*}{a_0 T_0} \right) + \ln \left( \frac{\rho_f^{1/4}}{H_1} \right) \right], \quad (33a)$$

$$T_{\text{re}} = \left( \frac{43}{11 g_{\text{s, re}}} \right)^{1/3} \left( \frac{a_0 H_1}{k_*} \right) e^{-(N_* + N_{\text{re}})} T_0, \quad (33b)$$

where  $T_0 = 2.725$  K is the present temperature of the CMB and  $H_0$  denotes the current value of the Hubble parameter. Moreover, note that,  $k_*/a_0$  represents the CMB pivot scale, with  $a_0$  denoting the scale factor today. We shall assume that  $k_*/a_0 \simeq 0.05 \text{ Mpc}^{-1}$ . We should also point out that  $N_*$  denotes the number of e-folds prior to the end of inflation when the pivot scale  $k_*$  leaves the Hubble radius.

## B. The case of perturbative reheating

As a second possibility, we shall consider the perturbative reheating scenario (for recent discussions, see, for instance, Refs. [91, 93]). In such a case, after inflation, the inflaton energy density, say,  $\rho_\phi$ , gradually decays into the radiation energy density, say,  $\rho_{\text{r}}$ , with the decay process being governed by the Boltzmann equations. As a result, the effective EoS parameter during the reheating phase becomes time dependent. In our analysis below, for simplicity, we shall assume that the EoS parameter  $w_\phi$  of the scalar field during the reheating phase remains constant. Such an assumption is valid as far as the oscillation time scale of the inflaton is much smaller than the Hubble time scale. This turns out to be generally true when the field is oscillating immediately after the end of inflation, and we should point out that such a behavior has also been seen in lattice simulations [116–118]. Hence, for a wide class of inflationary potentials which behave as  $V(\phi) \propto \phi^{2n}$  near the minimum, the time averaged EoS parameter of the inflaton can be expressed as  $w_\phi = (n-1)/(n+1)$  [119]. We should emphasize that this scenario is different from the one considered in the previous section wherein the explicit decay of the inflaton field was not taken into account. Specifically, in the earlier case, the energy density of the inflaton was supposed to be converted instantaneously into the energy density of radiation at a given time, leading to the end of the phase of reheating. In due course, we shall demonstrate the manner in which the detailed mechanism of reheating leaves specific imprints on the spectrum of primordial GWs observed today.

Let us define the following dimensionless variables to describe the comoving energy densities of the scalar field and radiation

$$\Phi(A) = \frac{\rho_\phi}{m_\phi^4} A^{3(1+w_\phi)}, \quad R(A) = \frac{\rho_{\text{r}}}{m_\phi^4} A^4, \quad (34)$$

where  $m_\phi$  denotes the mass of the inflaton. Also, let  $\Gamma_\phi$  represent the decay rate of the inflaton to radiation. In such a case, the Boltzmann equations governing the evolution of the energy densities  $\rho_\phi$  and  $\rho_R$  can be expressed as [91, 93, 120]

$$\frac{d\Phi}{dA} + \frac{\sqrt{3} M_{\text{Pl}} \Gamma_\phi}{m_\phi^2} (1 + w_\phi) \frac{A^{1/2} \Phi}{(\Phi/A^{3w_\phi}) + (R/A)} = 0, \quad (35a)$$

$$\frac{dR}{dA} - \frac{\sqrt{3} M_{\text{Pl}} \Gamma_\phi}{m_\phi^2} (1 + w_\phi) \frac{A^{3(1-2w_\phi)/2} \Phi}{(\Phi/A^{3w_\phi}) + (R/A)} = 0. \quad (35b)$$

Note that the tensor transfer function  $\chi_k$  is essentially governed by the behavior of the Hubble parameter  $H$  [cf. Eq. (25)]. It proves to be difficult to solve the above set of equations analytically. Therefore, to arrive at the Hubble parameter during the epoch of reheating, we shall solve the Boltzmann equations (35) numerically with the following conditions imposed at the end of inflation:

$$\rho_\phi(A=1) = \rho_f = \frac{3}{2} V_f, \quad \rho_R(A=1) = 0, \quad (36)$$

where, recall that,  $V_f$  is the value of the inflationary potential at the end of inflation. We should point out that, for the inflationary potential (13) of our interest,  $V_f$  is given by Eq. (18).

We should also clarify a couple of points in this regard. In the case of perturbative reheating, the phase of reheating is assumed to be complete when  $H = \Gamma_\phi$ . In other words, we require

$$H^2(A_{\text{re}}) = \frac{1}{3 M_{\text{Pl}}^2} [\rho_\phi(A_{\text{re}}, n_s, \Gamma_\phi) + \rho_R(A_{\text{re}}, n_s, \Gamma_\phi)] = \Gamma_\phi^2, \quad (37)$$

where  $A_{\text{re}} = a_{\text{re}}/a_f$ , with  $a_{\text{re}}$  denoting the scale factor when reheating has been achieved. In fact, this corresponds to the point in time when the rate of transfer of the energy from the inflaton to radiation is the maximum. The associated reheating temperature can then be determined from the energy density of radiation  $\rho_R$  through the relation

$$T_{\text{re}} = \left( \frac{30}{\pi^2 g_{r,\text{re}}} \right)^{1/4} \rho_R^{1/4}(A_{\text{re}}, n_s, \Gamma_\phi). \quad (38)$$

In fact, later, to arrive at the results on the spectrum of GWs today, along with specific values for the parameters describing the inflationary potential (that are consistent with the CMB data), we shall also choose a value of  $T_{\text{re}}$ . Having fixed the value of  $T_{\text{re}}$ , we shall make use of Eq. (33b) to arrive at  $N_{\text{re}}$  and thereby determine the value  $\Gamma_\phi$  using the condition  $H(A_{\text{re}}) = \Gamma_\phi$ .

With the solutions to the coupled background equations (35) at hand, we shall proceed to solve the differential equation (25) for the transfer function  $\chi_k$  during reheating. To illustrate the nature of the solutions, we have plotted the behavior of the Hubble parameter  $H$  and the transfer function  $\chi_k$  in Fig. 1 during the period of perturbative reheating. We have chosen specific values for the EoS parameter  $w_\phi$ , the reheating temperature  $T_{\text{re}}$ , and wave number  $k$  in plotting the figures. We have considered a wave number so that the mode reenters the Hubble radius during the period of reheating. As one would have expected, while the amplitude of the transfer function is a constant on super-Hubble scales, it decreases as the mode reenters the Hubble radius and begins to oscillate once inside.

#### IV. EVOLUTION DURING RADIATION DOMINATION AND THE SPECTRUM OF GWS TODAY

The Hubble parameter during the radiation dominated epoch evolves as

$$H^2 = H_{\text{re}}^2 \frac{A_{\text{re}}^4}{A^4} \quad (39)$$

with  $H_{\text{re}}$  and  $A_{\text{re}}$  denoting the Hubble parameter and the rescaled scale factor at the end of reheating, respectively. During radiation domination, the transfer function is governed by the equation

$$\frac{d^2 \chi_k}{dA^2} + \frac{2}{A} \frac{d\chi_k}{dA} + \frac{(k/k_{\text{re}})^2}{A_{\text{re}}^2} \chi_k = 0, \quad (40)$$

where  $k_{\text{re}} = a_{\text{re}} H_{\text{re}}$  is the mode which reenters the Hubble radius at the end of the reheating era. The above differential equation can be immediately solved to arrive at the following general solution:

$$\chi_k^{\text{RD}}(A) = \frac{1}{A} \left\{ E_k e^{-i(k/k_{\text{re}})[(A/A_{\text{re}})-1]} + F_k e^{i(k/k_{\text{re}})[(A/A_{\text{re}})-1]} \right\}. \quad (41)$$



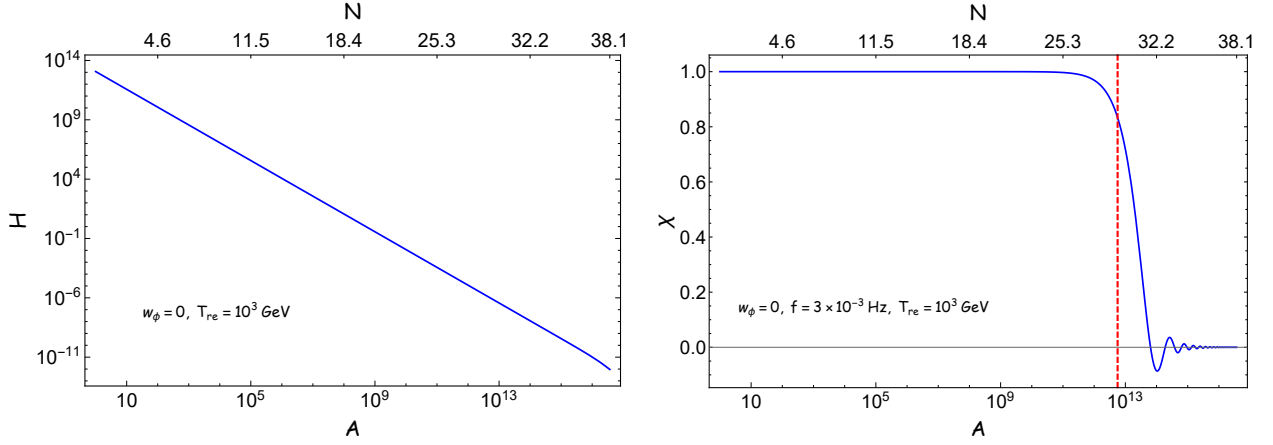


FIG. 1. The evolution of the Hubble parameter  $H$  (in blue, on the left) and the amplitude of the tensor transfer function  $\chi_k$  for a given wave number (in blue, on the right), obtained numerically in the case of the perturbative reheating scenario, have been plotted as a function of  $A = a/a_f$  over the domain  $1 \leq A \leq A_{\text{re}}$ , which corresponds to the period of reheating. We have also indicated the lapse in time in terms of e-folds (counted from the end of inflation) on the top of the two figures. We have assumed that  $w_\phi = 0$  and have set  $T_{\text{re}} = 10^3 \text{ GeV}$  in plotting the quantities. We have chosen the wave number to be  $k \simeq 2 \times 10^{12} \text{ Mpc}^{-1}$ , which corresponds to the frequency of  $f \simeq 3 \times 10^{-3} \text{ Hz}$  [cf. Eq. (1)]. The wave number has been chosen so that it reenters the Hubble radius during the epoch of reheating. The slope of the straight line describing  $H(A)$  (on the left) is  $-3/2$ , which is consistent with  $w_\phi = 0$ . We find that the slope changes as  $A$  approaches  $A_{\text{re}}$  indicating the beginning of the transition to the radiation dominated epoch. The vertical line (in red, on the right) indicates the time when the mode reenters the Hubble radius. As expected, the transfer function proves to be constant on super-Hubble scales and it oscillates once the mode is inside the Hubble radius.

The coefficients  $E_k$  and  $F_k$  need to be determined by matching this solution and its derivative with the solution (29) during the epoch of reheating and its derivative at  $A = A_{\text{re}}$ . Upon carrying out the matching at the junction between the eras of reheating and the radiation domination, we find that the coefficients  $E_k$  and  $F_k$  can be expressed as

$$E_k = \frac{A_{\text{re}}}{2} \left[ \left( 1 + \frac{i k_{\text{re}}}{k} \right) \chi_k^{\text{RH}}(A_{\text{re}}) + \frac{i k_{\text{re}}}{k} A_{\text{re}} \frac{d\chi_k^{\text{RH}}(A_{\text{re}})}{dA} \right] = i \frac{A_{\text{re}}}{2} \frac{k_{\text{re}}}{k} \mathcal{E}_k, \quad (42a)$$

$$F_k = \frac{A_{\text{re}}}{2} \left[ \left( 1 - \frac{i k_{\text{re}}}{k} \right) \chi_k^{\text{RH}}(A_{\text{re}}) - \frac{i k_{\text{re}}}{k} A_{\text{re}} \frac{d\chi_k^{\text{RH}}(A_{\text{re}})}{dA} \right] = -i \frac{A_{\text{re}}}{2} \frac{k_{\text{re}}}{k} \mathcal{F}_k, \quad (42b)$$

where we have also introduced the quantities  $\mathcal{E}_k$  and  $\mathcal{F}_k$  which we shall make use of later. At this stage, we should mention that the quantities  $\chi_k^{\text{RH}}(A_{\text{re}})$  and  $d\chi_k^{\text{RH}}(A_{\text{re}})/dA$  and hence the coefficients  $E_k$  and  $F_k$  will depend on the details of the reheating mechanism. In particular, they will be different for two the types of reheating mechanisms under consideration.

Since we have set  $h_k = h_k^{\text{P}} \chi_k$ , where  $h_k^{\text{P}}$  denotes the primordial amplitude of the tensor perturbations [cf. Eq. (21)], the energy density of GWs  $\rho_{\text{GW}}(k, \eta)$  is given by [cf. Eq. (23)]

$$\rho_{\text{GW}}(k, \eta) = \frac{M_{\text{Pl}}^2}{a^2} \frac{k^3}{2\pi^2} |h_k^{\text{P}}|^2 \left( \frac{1}{2} |\chi_k^{\text{RD}'(\eta)}|^2 + \frac{k^2}{2} |\chi_k^{\text{RD}}(\eta)|^2 \right). \quad (43)$$

On using the definition (7) of the inflationary tensor power spectrum  $\mathcal{P}_{\text{T}}(k)$ , this energy density of GWs can be expressed as

$$\rho_{\text{GW}}(k, \eta) = \frac{M_{\text{Pl}}^2}{4a^2} \mathcal{P}_{\text{T}}(k) \left( \frac{1}{2} |\chi_k^{\text{RD}'(\eta)}|^2 + \frac{k^2}{2} |\chi_k^{\text{RD}}(\eta)|^2 \right). \quad (44)$$

Upon substituting the solution (41) in the above expression, we obtain  $\rho_{\text{GW}}(k, \eta)$  to be

$$\begin{aligned} \rho_{\text{GW}}(k, \eta) = & \frac{M_{\text{Pl}}^2 k^2}{8a_f^2 A^4} \mathcal{P}_{\text{T}}(k) \left\{ (|E_k|^2 + |F_k|^2) \left[ 2 + \left( \frac{k_{\text{re}} A_{\text{re}}}{k A} \right)^2 \right] \right. \\ & \left. + E_k F_k^* \left( \frac{k_{\text{re}} A_{\text{re}}}{k A} \right)^2 \left( 1 + \frac{2i k A}{k_{\text{re}} A_{\text{re}}} \right) e^{-2i(k/k_{\text{re}})[(A/A_{\text{re}})-1]} \right\} \end{aligned}$$

$$+ E_k^* F_k \left( \frac{k_{\text{re}} A_{\text{re}}}{k A} \right)^2 \left( 1 - \frac{2 i k A}{k_{\text{re}} A_{\text{re}}} \right) e^{2 i (k/k_{\text{re}}) [(A/A_{\text{re}})-1]} \Big\}. \quad (45)$$

We had mentioned earlier that we shall be interested in the range of wave numbers which reenter the Hubble radius during the epochs of reheating and radiation domination. At late times during radiation domination such that  $A/A_{\text{re}} \gg 1$ , all the modes of our interest would be well inside the Hubble radius, i.e.  $k A \gg 1$ . In such a case, we find that, the above expression for  $\rho_{\text{GW}}(k, \eta)$  simplifies to be

$$\rho_{\text{GW}}(k, \eta) = \frac{M_{\text{Pl}}^2 k^2}{4 a_{\text{f}}^2 A^4} \mathcal{P}_{\text{T}}(k) (|E_k|^2 + |F_k|^2). \quad (46)$$

Hence, the corresponding dimensionless parameter describing the energy density of GWs, viz.  $\Omega_{\text{GW}}(k, \eta)$ , is given by

$$\Omega_{\text{GW}}(k, \eta) = \frac{k^2}{12 a_{\text{f}}^2 H^2 A^4} \mathcal{P}_{\text{T}}(k) (|E_k|^2 + |F_k|^2) = \frac{k_{\text{re}}^2 A_{\text{re}}^2}{48 a_{\text{f}}^2 H^2 A^4} \mathcal{P}_{\text{T}}(k) (|\mathcal{E}_k|^2 + |\mathcal{F}_k|^2), \quad (47)$$

where we have made use of the expressions (42) relating the coefficients  $E_k$  and  $F_k$  to the quantities  $\mathcal{E}_k$  and  $\mathcal{F}_k$ . During radiation domination,  $H^2 A^4 = H_{\text{re}}^2 A_{\text{re}}^4$ . Also, recall that,  $k_{\text{re}} = a_{\text{re}} H_{\text{re}}$ . On using these relations, at late times during radiation domination, we obtain that

$$\Omega_{\text{GW}}(k, \eta) = \frac{\mathcal{P}_{\text{T}}(k)}{48} (|\mathcal{E}_k|^2 + |\mathcal{F}_k|^2). \quad (48)$$

The task that remains is to explicitly determine the quantities  $\mathcal{E}_k$  and  $\mathcal{F}_k$ . In the special case of instantaneous reheating,  $A_{\text{re}} = 1$  and  $k_{\text{re}} = k_{\text{f}}$ . Therefore, on using the conditions (26) and (27), one can readily show that

$$\mathcal{E}_k = \frac{1 - 2 i (k/k_{\text{f}}) - 2 (k^2/k_{\text{f}}^2)}{1 - i (k/k_{\text{f}})}, \quad \mathcal{F}_k = \frac{1}{1 - i (k/k_{\text{f}})}. \quad (49)$$

For  $k \ll k_{\text{f}}$ , we find that,  $\mathcal{E}_k \simeq \mathcal{F}_k \simeq 1$ , which lead to

$$\Omega_{\text{GW}}(k, \eta) = \frac{\mathcal{P}_{\text{T}}(k)}{24} = \frac{H_{\text{r}}^2}{12 \pi^2 M_{\text{Pl}}^2}, \quad (50)$$

where, in arriving at the final expression, we have made use of the scale invariant inflationary tensor power spectrum (12). In other words, the dimensionless density parameter  $\Omega_{\text{GW}}(k, \eta)$  is strictly scale invariant over all wave numbers in the instantaneous reheating scenario. Evidently, such a behavior can be expected to hold true even when we have an epoch of reheating with  $w_{\phi} = 1/3$ , a result we shall encounter in due course.

Note that the energy density of GWs behaves as  $a^{-4}$  [cf. Eq. (46)], exactly as the energy density of radiation does. Such a behavior should not come as a surprise and it arises due to the fact that the modes of interest are well inside the Hubble radius at late times (say, close to the epoch of radiation-matter equality) during radiation domination. On utilizing this property, the dimensionless energy density parameter  $\Omega_{\text{GW}}(k)$  *today* can be expressed in terms of  $\Omega_{\text{GW}}(k, \eta)$  as follows:

$$\Omega_{\text{GW}}(k) h^2 = \left( \frac{g_{r,\text{eq}}}{g_{r,0}} \right) \left( \frac{g_{s,0}}{g_{s,\text{eq}}} \right)^{4/3} \Omega_{\text{R}} h^2 \Omega_{\text{GW}}(k, \eta) \simeq \left( \frac{g_{r,0}}{g_{r,\text{eq}}} \right)^{1/3} \Omega_{\text{R}} h^2 \Omega_{\text{GW}}(k, \eta), \quad (51)$$

where  $\Omega_{\text{R}}$  denotes the present day dimensionless energy density of radiation. We should mention that, while  $g_{r,\text{eq}}$  and  $g_{r,0}$  represent the number of relativistic degrees of freedom at equality and today, respectively,  $g_{s,\text{eq}}$  and  $g_{s,0}$  represent the number of such degrees of freedom that contribute to the entropy at these epochs. Further, the Hubble parameter today, as usual, has been expressed as  $H_0 = 100 h \text{ km sec}^{-1} \text{ Mpc}^{-1}$ .

The spectrum of primordial GWs in the reheating scenario with an averaged EoS parameter can be expected to be different when compared to the one arising in the perturbative reheating scenario. In the following two sections, we shall derive the spectrum of primordial GWs at the present epoch in the two cases.

## V. SPECTRUM OF GWS IN REHEATING DESCRIBED BY AN AVERAGED EOS PARAMETER

Before we go on to discuss the results, we should mention that the spectrum of GWs arising in the scenario wherein the epoch of reheating is described by an averaged EoS parameter and the transition to radiation domination is

assumed to occur instantaneously at a given time has been evaluated earlier in the literature (see, for instance, Refs. [62, 65, 71]; for a recent discussion, see Ref. [80]). However, we find that, in the earlier investigations, the initial conditions that determine the dynamics during reheating have not always been chosen to be consistent with the dynamics during inflation. In this work, we shall consider a specific model of inflation and we shall show that model dependent initial conditions play a primary role in determining the range of frequencies which reenter the Hubble radius during reheating. Therefore, in this section, we shall reanalyze the effect of the averaged EoS parameter during reheating (with appropriate initial conditions) on the spectrum of GWs. We shall briefly discuss the derivation of the spectrum of GWs and arrive at the shape of the spectrum in the domains  $k < k_{\text{re}}$  and  $k > k_{\text{re}}$ . In the next section, we shall compare the results with those that arise in the case of perturbative reheating.

It should be clear from the expression (48) that we shall require the quantities  $\mathcal{E}_k$  and  $\mathcal{F}_k$  to arrive at the spectrum of GWs. Using Eqs. (42), we can express  $\mathcal{E}_k$  and  $\mathcal{F}_k$  as

$$\mathcal{E}_k = \left(1 - \frac{ik}{k_{\text{re}}}\right) \chi_k^{\text{RH}}(A_{\text{re}}) + A_{\text{re}} \frac{d\chi_k^{\text{RH}}(A_{\text{re}})}{dA}, \quad (52a)$$

$$\mathcal{F}_k = \left(1 + \frac{ik}{k_{\text{re}}}\right) \chi_k^{\text{RH}}(A_{\text{re}}) + A_{\text{re}} \frac{d\chi_k^{\text{RH}}(A_{\text{re}})}{dA}. \quad (52b)$$

Also, recall that the transfer function at the end of the epoch of reheating  $\chi_k^{\text{RH}}(A_{\text{re}})$  is given by Eq. (29), with the coefficients  $C_k$  and  $D_k$  being described by Eqs. (31). During radiation domination, we have  $H^2 A^4 = H_{\text{re}}^2 A_{\text{re}}^4$ . Since  $k_{\text{f}} = a_{\text{f}} H_{\text{f}}$  and  $k_{\text{re}} = a_{\text{re}} H_{\text{re}}$ , we find that we can write  $A_{\text{re}} = (k_{\text{f}}/k_{\text{re}})^{1/\gamma}$ . As a result, the Bessel functions in the expression (29) for  $\chi_k^{\text{RH}}(A_{\text{re}})$  depend on the ratio  $(k/k_{\text{re}})$ . Note that, in contrast, the coefficients  $C_k$  and  $D_k$  depend only on the ratio  $k/k_{\text{f}}$ . As we mentioned earlier, we have been interested in arriving at the spectrum over wave numbers such that  $k < 10^{-2} k_{\text{f}}$ . For small  $z$ , the Bessel function  $J_\alpha(z)$  behaves as (see, for instance, Ref. [121])

$$\lim_{z \ll 1} J_\alpha(z) \simeq \frac{1}{\Gamma(1 + \alpha)} \left(\frac{z}{2}\right)^\alpha, \quad (53)$$

where  $\Gamma(z)$  denotes the Gamma function. Clearly, in such a limit, the Bessel functions involving the largest negative value for the index  $\alpha$  can be expected to dominate. Since  $0 \leq w_\phi \leq 1$ , the quantities  $\nu$  and  $\gamma$  are always positive [cf. Eq. (30)]. Hence, in the limit  $k \ll k_{\text{f}}$ , we find that it is the term involving  $D_k$  in Eq. (29) that will dominate. For the above reasons, the quantity  $\chi_k^{\text{RH}}(A_{\text{re}})$  can be approximated as follows:

$$\chi_k^{\text{RH}}(A_{\text{re}}) \simeq A_{\text{re}}^{-\nu} D_k J_{\nu/\gamma} \left(\frac{k}{\gamma k_{\text{re}}}\right), \quad (54)$$

with the coefficient  $D_k$  being given by

$$D_k \simeq -\frac{\pi}{\Gamma(-\nu/\gamma)} \csc \left(\frac{\pi\nu}{\gamma}\right) \left(\frac{k}{2\gamma k_{\text{f}}}\right)^{-\nu/\gamma}. \quad (55)$$

Let us first arrive at the shape of the spectrum in the domain  $k \ll k_{\text{re}}$ . In such a domain, we can use the form (53) for the Bessel function  $J_{\nu/\gamma}[k/(\gamma k_{\text{re}})]$  that appears in the expression (54) above for  $\chi_k^{\text{RH}}(A_{\text{re}})$ . On doing so and utilizing the identity  $\Gamma(z)\Gamma(1-z) = \pi/\sin(\pi z)$  [121], we find that, in the domain  $k \ll k_{\text{re}}$ , the quantity  $\chi_k^{\text{RH}}(A_{\text{re}})$  reduces to unity. Under the same conditions, we find that the quantity  $d\chi_k^{\text{RH}}(A_{\text{re}})/dA$  vanishes. Therefore, it should be evident from the expressions (52) that, in the limit  $k \ll k_{\text{re}}$ ,  $\mathcal{E}_k \simeq \mathcal{F}_k \simeq 1$ . In other words, the spectrum of GWs today is scale invariant over this domain and its present day amplitude is given by

$$\Omega_{\text{GW}}(k) h^2 \simeq \left(\frac{g_{r,0}}{g_{r,\text{eq}}}\right)^{1/3} \Omega_{\text{r}} h^2 \frac{\mathcal{P}_{\text{T}}(k)}{24} \simeq \Omega_{\text{r}} h^2 \frac{H_{\text{f}}^2}{12\pi^2 M_{\text{pl}}^2}. \quad (56)$$

In arriving at the final expression, we have assumed that  $g_{r,0} \simeq g_{r,\text{eq}}$  and have made use of the tensor power spectrum (12) arising in de Sitter inflation. We should mention that this result is the same as in the case of instantaneous reheating. This result should come as a surprise since these large scale modes are on super-Hubble scales during the epoch of reheating and hence are not influenced by it.

Let us now turn to the domain  $k \gg k_{\text{re}}$ . Since the limit  $k \ll k_{\text{f}}$  continues to be valid, the term involving  $D_k$  in Eq. (29) remains the dominant term. Therefore,  $\chi_k^{\text{RH}}(A_{\text{re}})$  is again described by Eq. (54), with  $D_k$  given by Eq. (55). However, the argument of the Bessel function in Eq. (54) is now large. For large  $z$ , the Bessel function  $J_\alpha(z)$  behaves as (see, for instance, Ref. [121])

$$\lim_{z \gg 1} J_\alpha(z) \simeq \sqrt{\frac{2}{\pi z}} \cos[z - \pi\alpha - (\pi/4)]. \quad (57)$$

Therefore, in the domain  $k \gg k_{\text{re}}$ , we find that the quantity  $\chi_k^{\text{RH}}(A_{\text{re}})$  and its derivative  $d\chi_k^{\text{RH}}(A_{\text{re}})/dA$  behave as

$$\chi_k^{\text{RH}}(A_{\text{re}}) \simeq -\frac{1}{\sqrt{\pi}} \Gamma\left(1 + \frac{\nu}{\gamma}\right) \left(\frac{k}{2\gamma k_{\text{re}}}\right)^{-(\nu/\gamma)-(1/2)} \cos\left(\frac{k}{2\gamma k_{\text{re}}} - \frac{\pi\nu}{\gamma} - \frac{\pi}{4}\right), \quad (58a)$$

$$A_{\text{re}} \frac{d\chi_k^{\text{RH}}(A_{\text{re}})}{dA} \simeq -\frac{2\gamma}{\sqrt{\pi}} \Gamma\left(1 + \frac{\nu}{\gamma}\right) \left(\frac{k}{2\gamma k_{\text{re}}}\right)^{-(\nu/\gamma)+(1/2)} \sin\left(\frac{k}{2\gamma k_{\text{re}}} - \frac{\pi\nu}{\gamma} - \frac{\pi}{4}\right), \quad (58b)$$

with  $\nu$  and  $\gamma$  being given by Eq. (30). On substituting these expressions in Eqs. (52), we obtain the corresponding  $\mathcal{E}_k$  and  $\mathcal{F}_k$  to be

$$\mathcal{E}_k \simeq \mathcal{F}_k^* \simeq -\frac{2i\gamma}{\sqrt{\pi}} \Gamma\left(1 + \frac{\nu}{\gamma}\right) \left(\frac{k}{2\gamma k_{\text{re}}}\right)^{-(\nu/\gamma)+(1/2)} \exp i\left(\frac{k}{2\gamma k_{\text{re}}} - \frac{\pi\nu}{\gamma} - \frac{\pi}{4}\right) \quad (59)$$

so that

$$|\mathcal{E}_k|^2 = |\mathcal{F}_k|^2 = \frac{4\gamma^2}{\pi} \Gamma^2\left(1 + \frac{\nu}{\gamma}\right) \left(\frac{k}{2\gamma k_{\text{re}}}\right)^{n_{\text{GW}}}, \quad (60)$$

where we have defined  $n_{\text{GW}}$  to be

$$n_{\text{GW}} = 1 - \frac{2\nu}{\gamma} = -\frac{2(1 - 3w_\phi)}{1 + 3w_\phi}. \quad (61)$$

If we substitute these results in the expression (51), we obtain the spectrum of GWs today in the domain  $k \gg k_{\text{re}}$  to be

$$\Omega_{\text{GW}}(k) h^2 \simeq \left(\frac{g_{r,0}}{g_{r,\text{eq}}}\right)^{1/3} \Omega_{\text{R}} h^2 \frac{\mathcal{P}_{\text{T}}(k)}{24} |\mathcal{E}_k|^2 \simeq \Omega_{\text{R}} h^2 \frac{H_1^2}{12\pi^2 M_{\text{Pl}}^2} \frac{4\gamma^2}{\pi} \Gamma^2\left(1 + \frac{\nu}{\gamma}\right) \left(\frac{k}{2\gamma k_{\text{re}}}\right)^{n_{\text{GW}}}. \quad (62)$$

In other words, for wave numbers such that  $k \gg k_{\text{re}}$ , the spectrum of GWs today has the index  $n_{\text{GW}}$ . Notably, the index vanishes when  $w_\phi = 1/3$ . Also, while the spectrum is blue for  $w_\phi > 1/3$ , it is red for  $w_\phi < 1/3$ . Moreover, in the extreme cases wherein  $w_\phi$  vanishes or is unity, we have  $n_{\text{GW}} = -2$  and  $n_{\text{GW}} = 1$ , respectively.

On utilizing the expression (29) for the transfer function during reheating and the expressions (42) to determine the quantities  $\mathcal{E}_k$  and  $\mathcal{F}_k$ , we can arrive at the complete spectrum of GWs by substituting the expressions in Eq. (48). In Fig. 2, we have plotted the spectrum of GWs today that arise in the case of the  $\alpha$ -attractor model (13) for a set of values of the EoS parameter  $w_\phi$ . In plotting the spectra, we have chosen the other parameters in such a fashion that the reheating temperature is  $T_{\text{re}} = 3\text{ GeV}$  in all the cases. The figure clearly illustrates the qualitative features we discussed above: (i) the spectrum is strictly scale invariant for  $k < k_{\text{re}}$ , and (ii) the spectrum has the index  $n_{\text{GW}}$  for  $k > k_{\text{re}}$ . We have plotted the spectra for  $w_\phi = (0, 1/3, 1/2, 2/3)$ , which correspond to the values  $n = (1, 2, 3, 5)$  for the index in the potential (13). We should mention that these cases lead to the indices  $n_{\text{GW}} = (-2, 0, 2/5, 2/3)$ , as expected. In the figure, we have also included the sensitivity curves of the some of the current and forthcoming GW observatories (for a discussion on the sensitivity curves, see Ref. [122] and the associated web-page). Interestingly, we find that, for a set of inflationary and reheating parameters, the spectra already intersect the sensitivity curves. Moreover, we find that the BBN bound, viz.  $\Omega_{\text{GW}}(k_{\text{f}}) h^2 \leq 10^{-6}$  (in this context, see, for instance, Ref. [123] and the reviews [17, 18]), can be violated for  $w_\phi > 1/3$ , which leads to constraints on the EoS parameter  $w_\phi$  for a given  $k_{\text{f}}$  and vice-versa. As we have emphasized, Fig. 2 depicts the interesting dependence of the value of  $k_{\text{f}}$  on the inflationary model parameter  $n$  due to different initial conditions at the beginning of reheating. This interdependence of  $k_{\text{f}}$  and the EoS parameter  $w_\phi$  can be translated into the constraints on the reheating temperature  $T_{\text{re}}$  and scalar spectral index  $n_{\text{s}}$  through the aforementioned BBN bound. For instance, in the figure, the spectrum corresponding to  $w_\phi = 2/3$  clearly crosses the BBN bound at large frequencies. These clearly suggest that observations of the spectrum of GWs today can lead to interesting constraints on the primordial physics.

## VI. SPECTRUM OF GWS IN THE CASE OF PERTURBATIVE REHEATING

In the perturbative reheating scenario, the inflaton continuously transfers its energy to radiation after the end of the inflationary epoch. As a result, the effective EoS parameter during the reheating era, say,  $w_{\text{eff}}$ , becomes time dependent. It can be expressed as

$$w_{\text{eff}} = \frac{3w_\phi \rho_\phi + \rho_{\text{R}}}{3(\rho_\phi + \rho_{\text{R}})}, \quad (63)$$

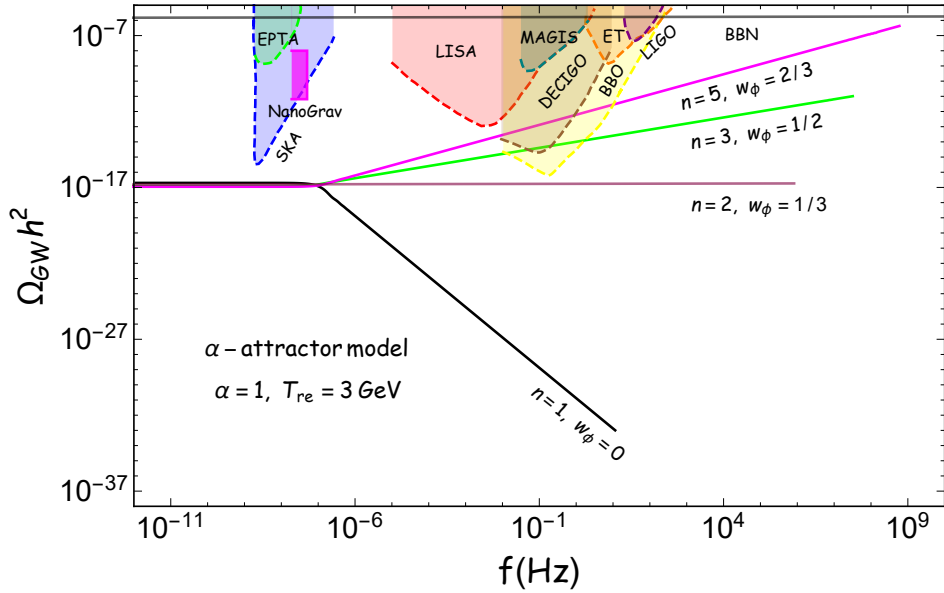


FIG. 2. The behavior of the dimensionless energy density of primordial GWs observed today, viz.  $\Omega_{\text{GW}}(f)$ , has been plotted over a wide range of frequencies. The spectrum has been obtained analytically and it corresponds to the case wherein the post-inflationary phase is described by the EoS parameter  $w_\phi$  and reheating is expected to occur instantaneously at a given time. We have considered the scenario wherein the inflationary potential is described by the  $\alpha$ -attractor model (13). We have illustrated the spectra for the cases wherein  $n = (1, 2, 3, 5)$  (in black, brown, green and magenta), which correspond to  $w_\phi = (0, 1/3, 1/2, 2/3)$ . We should mention that we have chosen the parameters such that  $T_{\text{re}} = 3 \text{ GeV}$  in all the cases. In the figure, we have also included the sensitivity curves of the different ongoing and forthcoming GW observatories (in varied colors, on top). Note that, as expected, the spectrum is strictly scale invariant for frequencies such that  $f < f_{\text{re}} = k_{\text{re}}/(2\pi)$ . However, for larger frequencies such that  $f > f_{\text{re}}$ , while the spectrum has a red tilt for  $w_\phi < 1/3$ , it has a blue tilt for  $w_\phi > 1/3$ . Interestingly, we find that, for a suitably large value of  $w_\phi$ , the spectrum of GWs already intersect the sensitivity curves of some of the observatories over a certain range of frequencies. Moreover, we find that, for a high value of  $w_\phi$ , the spectra cross the BBN bound of  $\Omega_{\text{GW}} h^2 < 10^{-6}$  at suitably large frequencies.

where, recall that, the evolution of the energy densities of the inflaton and radiation, viz.  $\rho_\phi$  and  $\rho_R$ , are governed by the Boltzmann equations (35), while  $w_\phi$  is the EoS parameter describing the inflaton. Such a time dependence of the effective EoS parameter has been explicitly demonstrated earlier (see, for example, Refs. [91, 93]). It has been illustrated that, while immediately after the termination of inflation,  $w_{\text{eff}}$  is approximately equal to  $w_\phi$ , after a certain time, the effective EoS parameter smoothly transits from  $w_\phi$  to  $1/3$ , which indicates the onset of the epoch of radiation domination. We should emphasize again here that such a reheating scenario is different from the case considered in the previous section where the inflaton energy density is assumed to be converted instantaneously into radiation after a certain period of time. Specifically, in the previous reheating scenario,  $w_{\text{eff}}$  remains equal to  $w_\phi$  during the whole of reheating era and, at a particular time,  $w_{\text{eff}}$  sharply changes to  $1/3$ . These differences in the dynamics of the reheating scenarios should be reflected in spectrum of GWs today. The corresponding features in the GW spectrum can, in principle, help us probe the microscopic mechanisms operating during the era of reheating.

We shall now proceed to compute the spectrum of GWs at the present time, i.e.  $\Omega_{\text{GW}}(k)$  or, equivalently,  $\Omega_{\text{GW}}(f)$ , in the case of the perturbative reheating scenario. As we had discussed, we shall analyze this case numerically. With the solution to the Hubble parameter  $H(A)$  at hand, we proceed to solve for the transfer function  $\chi_k(A)$  during the epoch of reheating, as we had outlined in section III. The numerical solutions are determined using the initial conditions (26) and (27). With the solutions at hand, we arrive at the spectrum of GWs at the current epoch for different sets of reheating temperature and the EoS parameter  $w_\phi$  describing the inflaton. The results we have obtained are illustrated in Figs. 3 and 4 for the cases of  $w_\phi < 1/3$  and  $w_\phi > 1/3$ , respectively. Let us now highlight a few points concerning the results plotted in the two figures.

Let us first broadly understand the spectra in Fig. 3 wherein we have plotted the results for  $w_\phi = 0$ . In the figure, we have illustrated the dimensionless energy density of GWs today as a function of the frequency  $f$ . We have considered the case wherein the inflationary potential is described by the  $\alpha$ -attractor model (13), and have plotted the results for  $n = 1$  (which corresponds to  $w_\phi = 0$ ) and a set of values of  $T_{\text{re}}$ . We have also included behavior of the effective EoS parameter  $w_{\text{eff}}$ , which we have plotted as a function of frequency using the relation  $f = aH/(2\pi)$ . The plot indicates the evolution of the parameter  $w_{\text{eff}}$  as the modes with different frequencies  $f$  reenter the Hubble

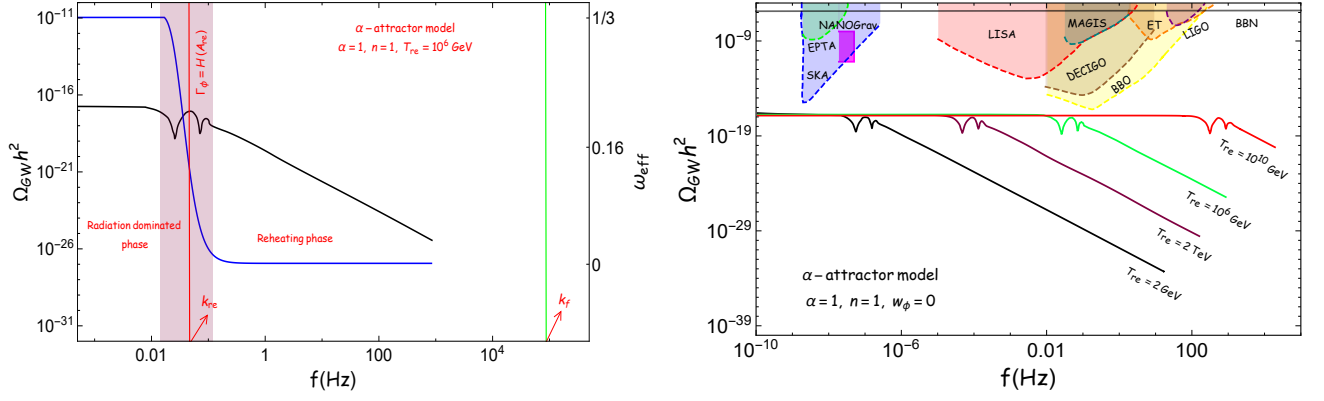


FIG. 3. The behavior of the dimensionless energy density of primordial GWs today, viz.  $\Omega_{\text{GW}}(f)$ , has been plotted over a small (in black, on the left) as well as a wide range of frequencies (in red, green, brown and black, on the right). We have considered the scenario wherein the inflationary potential is described by the  $\alpha$ -attractor model (13) with  $n = 1$ , which corresponds to  $w_\phi = 0$ . We have plotted the spectrum of GWs for the following values of the reheating temperature  $T_{\text{re}}$ :  $10^{10}$  GeV (in red, on the right),  $10^6$  GeV (in black on the left and green on the right), 2 TeV and 2 GeV (in brown and black on the right). Note that, we have also illustrated the behavior of the effective EoS parameter  $w_{\text{eff}}$  (in blue, in the figure on the left) as a function of the frequency  $f$ , which has been determined using the relation  $f = aH/(2\pi)$ . In other words,  $w_{\text{eff}}(f)$  (marked on the  $y$ -axis on the right hand side of the figure on the left) represents the effective EoS parameter at the instant when the mode with the frequency  $f$  reenters the Hubble radius. We have also indicated the frequencies associated with the wave numbers  $k_{\text{re}}$  and  $k_{\text{f}}$  (as vertical red and green lines, on the left). Moreover, we have demarcated the regime (in pink) wherein the transition from  $w_{\text{eff}} = 0$  to  $w_{\text{eff}} = 1/3$  occurs. We should point out that the spectrum of GWs exhibit oscillations in the region of the transition. Further, we have included the sensitivity curves of different ongoing and forthcoming GW observatories (in the figure on the right).

radius (in this context, also see the earlier efforts [91, 93]). Note that larger wave numbers or, equivalently, larger frequencies reenter the Hubble radius earlier than the smaller ones. The plot clearly highlights the transition from the inflaton dominated universe to the epoch of radiation domination, achieved through the mechanism of perturbative reheating. The transition is clearly reflected in the behavior of the effective EoS parameter which changes smoothly from  $w_{\text{eff}} = 0$  at early times (i.e. at large frequencies) to  $w_{\text{eff}} = 1/3$  at late times (i.e. at small frequencies). In the figure, we have indicated the frequencies associated with the wave numbers  $k_{\text{f}}$  and  $k_{\text{re}}$  and have also marked the domain of the transition to highlight these points.

Let us now point out a few more aspects of the results presented in Fig. 3. In the figure, we have also plotted the spectrum of GWs for a few different values of the reheating temperature. Further, we have included the sensitivity curves of different current and forthcoming GW observatories. Note that the plots suggest that the spectra of GWs remain scale invariant over wave numbers  $k < k_{\text{re}}$  which reenter the Hubble radius during the radiation dominated epoch. This result should not come as surprise. As we have pointed out earlier, these modes are on super-Hubble scales during the period of reheating and hence are unaffected by the process. Therefore, they carry the scale invariant nature of the spectrum of GWs generated during inflation. However, modes with wave numbers  $k_{\text{re}} < k < k_{\text{f}}$  reenter the Hubble radius during the epoch of reheating and hence they carry the signatures of the mechanism of reheating. For the value of  $w_\phi = 0$  we have worked with in Fig. 3, we find that the spectrum exhibits a strong red tilt for  $k > k_{\text{re}}$ . In fact, we find that the red tilt occurs over this range of wave numbers whenever  $w_\phi < 1/3$ . Moreover, for lower values of the reheating temperature, the epoch of reheating lasts longer. Since reheating is delayed, the mode with wave number  $k_{\text{re}}$  reenters the Hubble radius at a later time or, equivalently, leaves the Hubble radius during inflation at an earlier time thereby suggesting that it will have a smaller wave number. We should mention here that these features in the spectrum of GWs are similar to the behavior in the simpler reheating scenario we had discussed in the last section.

Interestingly, we find that the perturbative reheating scenario leaves tell tale imprints on the spectrum of GWs which can possibly help us decipher finer details of the mechanism of reheating. We find that the spectrum exhibits a burst of oscillations near  $k_{\text{re}}$ . It should be clear from Fig. 3 that the oscillations occur over modes which leave the Hubble radius during the period of the transition when  $w_{\text{eff}}$  changes from its initial value of  $w_\phi$  to the final value of  $1/3$ . Recall that, in the perturbative reheating scenario, the reheating temperature is identified as the temperature associated with the energy density of radiation at the instance when  $H(A_{\text{re}}) = \Gamma_\phi$ . Consequently, it is at this point of time that the change in the effective EoS parameter with respect to the scale factor is the maximum. This aspect is



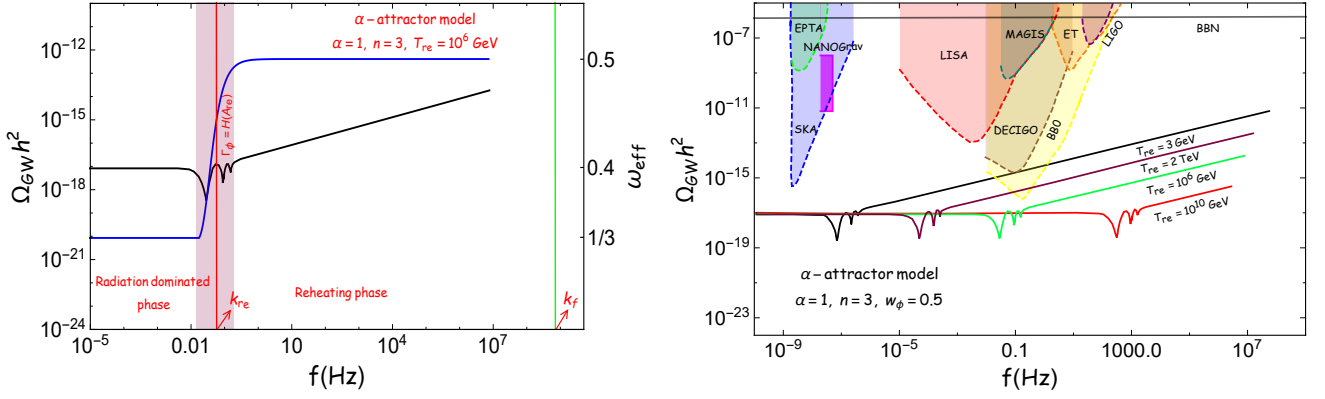


FIG. 4. The spectrum of GWs today have been illustrated in the same manner as in the last figure. But, in contrast to the previous figure wherein we had considered the case  $w_\phi = 0$  [or, equivalently,  $n = 1$  in the potential (13)], we have set  $w_\phi = 0.5$  (i.e.  $n = 3$ ) in arriving at the plots above. Note that, as in the case of  $w_\phi = 0$ , the spectrum is scale invariant over frequencies corresponding to  $k < k_{\text{re}}$ . However, the spectrum spectrum has a strong blue tilt at higher frequencies. Importantly, for some values of the reheating temperature, the spectra intersect the sensitivity curves of the various GW observatories which immediately translate to constraints on the parameters  $w_\phi$  and  $T_{\text{re}}$  that characterize the epoch of reheating. In the figure, we have also included the BBN constraint (as the horizontal black line, on the right), which corresponds to  $\Omega_{\text{GW}} h^2 < 10^{-6}$ .

reflected in the peak that arises in the spectrum of GWs exactly at the wave number  $k_{\text{re}}$  which re-enters the Hubble radius when  $H(A_{\text{re}}) = \Gamma_\phi$ . We should also mention that these features in the spectrum of GWs spectrum are not limited only to the case of  $w_\phi = 0$  and  $T_{\text{re}} = 10^6$  GeV, but also arise for all possible sets of values of  $(w_\phi < 1/3, T_{\text{re}})$ . In order to highlight this point, in Fig. 3, we have illustrated the spectrum  $\Omega_{\text{GW}}(f)$  for different values of reheating temperature  $T_{\text{re}}$ . However, note that, the frequency around which the spectrum begins to exhibit a red tilt increases as the reheating temperature increases. This is expected for the reason we discussed above, viz. that the period of reheating is shorter for a higher reheating temperature as a result of which the wave number  $k_{\text{re}}$  of the mode which re-enters the Hubble radius at the end of reheating turns out to be larger. Lastly, we should mention that, for  $w_\phi < 1/3$ , the spectrum of GWs is indeed compatible with the BBN constraints.

To illustrate the dependence of the spectrum of GWs on  $w_\phi$ , in Fig. 4, we have plotted the spectrum for  $w_\phi = 1/2$  [i.e. for  $n = 3$  in the potential (13)] and a set of values of the reheating temperature, just as in Fig. 3. Clearly, the spectrum of GWs is scale invariant over frequencies corresponding to  $k < k_{\text{re}}$ . But, in contrast to the  $w_\phi = 0$  case, the spectrum has a strong blue tilt at higher frequencies. Also, as expected, the higher the reheating temperature, the larger is  $k_{\text{re}}$ , for reasons we have discussed earlier. Moreover, we find that the spectrum exhibits a burst of oscillation around  $k_{\text{re}}$ , exactly as in the  $w_\phi = 0$  case. Further, the maximum of the oscillation occurs at the instance when  $k_{\text{re}}$  reenters the Hubble radius and the width of the oscillation coincides with the period of transition from  $w_{\text{eff}} = w_\phi = 0.5$  to  $w_{\text{eff}} = 1/3$ . Finally, we should mention that the spectra exhibit a blue tilt for  $k > k_{\text{re}}$  whenever  $w_\phi > 1/3$ .

The above arguments clearly indicate that the details of epoch of reheating significantly affects the spectrum of GWs. Therefore, the characteristic features of  $\Omega_{\text{GW}}(f)$  can considerably aid us in garnering adequate amount of information regarding the reheating phase. Upon comparing Figs. 2 and 3 (or 4), it is clear that the perturbative reheating mechanism, wherein the transfer of energy from the inflaton to radiation occurs smoothly, leads to oscillations in the spectrum of GWs in contrast to the simpler model wherein the transition to radiation domination occurs instantaneously. We believe that such quantitative differences can provide us with stronger constraints on the mechanism of reheating. Specifically,

- The presence of the oscillating feature in the spectrum of GWs, in particular, the width of the oscillation can provide us information concerning the time scale over which  $w_{\text{eff}}$  makes the transition from  $w_\phi$  to  $1/3$ .
- As we have discussed above, the peak of the oscillation occurs at  $k = k_{\text{re}}$ . Thus, identifying the location of the peak of the oscillation in the spectrum can help us determine the Hubble scale at the end of reheating or, equivalently, the decay rate  $\Gamma_\phi$  of the inflaton to radiation. In other words, the observation of the peak can indicate the strength of the coupling between the inflaton and radiation in a given a decay channel.

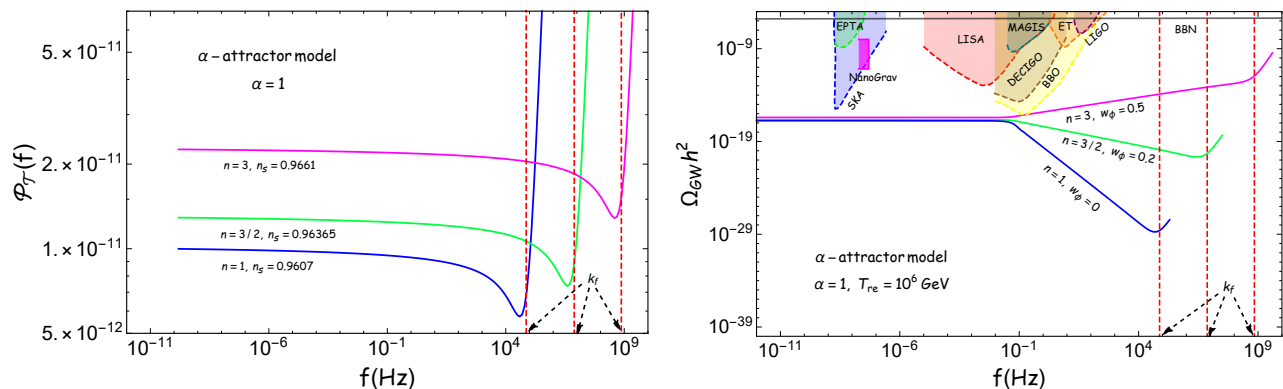


FIG. 5. The inflationary tensor power spectrum arising in the  $\alpha$ -attractor model of interest (on the left) as well as the corresponding spectrum of GWs today (on the right) have been plotted for frequencies close to the wave number  $k_f$ . The inflationary spectra have been computed numerically and we have made use of the analytical solutions for the tensor transfer function  $\chi_k$  during the post-inflationary epochs to arrive at the spectrum of GWs today. We have plotted the spectrum of GWs today, viz.  $\Omega_{\text{GW}}(f)$ , for a few different values of the reheating EoS parameter  $w_\phi$  and a specific reheating temperature. We find that, while the inflationary power spectrum begins to behave as  $k^2$  near  $k_f$ , the corresponding spectra of GWs today behave as  $k^4$ .

## VII. SPECTRUM OF GWS NEAR THE END OF THE INFLATION

Until now, while discussing the tensor power spectrum generated during inflation, for simplicity, we had assumed that inflation was of the de Sitter form. This had led to a scale invariant power spectrum for scales such that  $k \ll k_f$  [cf. Eq. (12)], where  $k_f$  denotes the wave number that leaves the Hubble radius at the end of inflation. However, potentials such as the  $\alpha$ -attractor model (13) of our interest actually lead to slow roll inflation and, as we had mentioned earlier, in such cases, there will arise a small tensor spectral tilt. Moreover, even the slow roll approximation will cease to be valid towards the end of inflation. Therefore, to understand the nature of the inflationary tensor power spectrum close to the wave number  $k_f$ , the easiest method seems to evaluate the spectrum numerically.

There exists a standard procedure to evaluate the spectrum of perturbations generated during inflation (in this context, see, for instance, Ref. [124]). The modes are typically evolved from the Bunch-Davies initial conditions when they are well inside the Hubble radius and the spectra are evaluated in the super-Hubble domain when the amplitude of the perturbations have frozen. Such an approach works well for the large scale modes. But, since we are interested in the tensor power spectrum over small scales, in particular, with wave numbers close to  $k_f$ , these modes would not be able to spend adequate amount of time in the super-Hubble regime. Hence, in these situations, the best approach would be evaluate the spectrum at the end of inflation. In Fig. 5, we have plotted the inflationary tensor power spectrum computed numerically in the  $\alpha$ -attractor model of our interest. Actually, in the figure, we have also plotted the spectra of GWs today  $\Omega_{\text{GW}}(f)$  for a few sets of values of the EoS parameter  $w_\phi$  and a specific value of the reheating temperature. Having computed the inflationary spectra numerically, we have used the analytical forms for the tensor transfer function post-inflation to arrive at the  $\Omega_{\text{GW}}(f)$ . Note that the inflationary spectral shape begins to change for wave numbers close to  $k_f$ . In fact, we find that, the inflationary tensor power spectrum  $\mathcal{P}_T(k)$  behaves as  $k^2$  for wave numbers close to and beyond  $k_f$ . This is not surprising and occurs due to the fact that these modes have either hardly left or remain inside the Hubble radius at the end of inflation. Therefore, the modes are essentially of the Minkowskian form leading to the  $k^2$  behavior of the power spectrum. From the structure of energy density of GWs [cf. Eq. (21)], it is easy to establish that the corresponding  $\Omega_{\text{GW}}(k)$  would behave as  $k^4$  over this domain of wave numbers. It is easy to see from Fig. 5 that  $\Omega_{\text{GW}}(f)$  indeed behaves as expected around and beyond  $k_f$ . Further, from the figure, we can see that  $k_f$  is crucially dependent on the structure of the inflationary potential. For reheating dynamics described by an effective EoS parameter  $w_\phi$ , we can write  $k_f$  in terms of the potential parameter  $n$ , the reheating parameters ( $T_{\text{re}} N_{\text{re}}$ ) and the inflationary parameter  $N_*$  as follows:

$$k_f = a_f H_f = k_* \frac{H_f}{H_1} e^{N_*} = k_* \left( \frac{V_f}{2 H_1^2 M_{\text{pl}}^2} \right)^{1/2} e^{N_*} = k_* \left( \frac{\pi^2 g_{r,\text{re}}}{90} \right)^{1/2} \frac{T_{\text{re}}^2}{H_1 M_{\text{pl}}} e^{N_* + [3n/(n+1)] N_{\text{re}}}, \quad (64)$$

where we have been careful to distinguish between the value of  $H_{k_*} \simeq H_1$  and  $H_f$ , i.e. the Hubble parameters evaluated at the moment when the pivot scale  $k_*$  crosses the Hubble radius and at the end of the inflation, respectively.

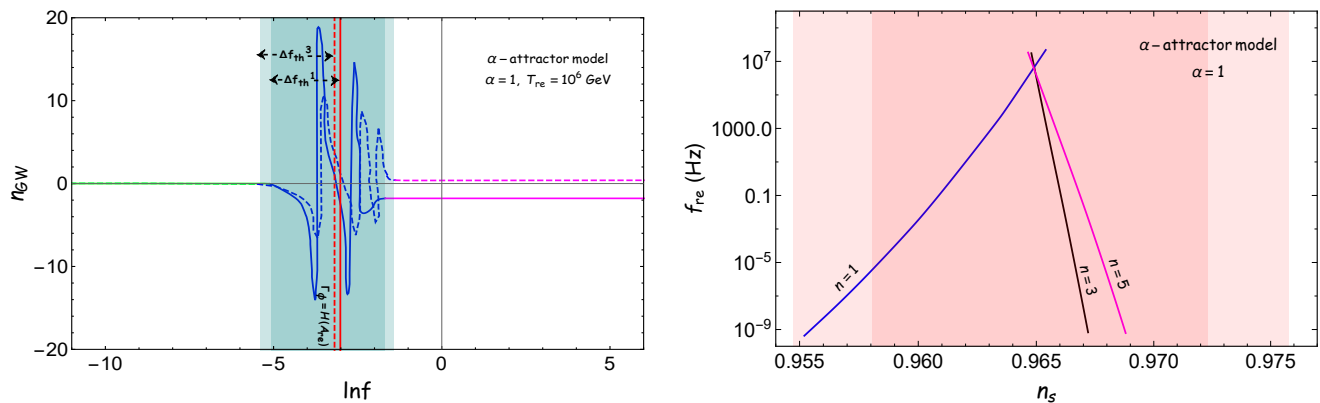


FIG. 6. *Left*: The variation of the index  $n_{\text{GW}}$  associated the spectrum of primordial GWs observed today in the case of the perturbative reheating scenario has been plotted as a function of frequency  $f$  for two different values of the inflaton EoS parameter  $w_\phi = (0, 1/2)$  (as solid and dashed lines) for the  $\alpha$ -attractor potential (13). We have fixed value of the reheating temperature to be  $T_{\text{re}} = 10^6$  GeV in arriving at the plot. In the figure (on the left), we have also explicitly highlighted the behavior of  $n_{\text{GW}}$  for modes that re-enter the Hubble radius during the following regimes: (i) reheating phase dominated by the inflaton (as solid and dashed lines, in magenta), (ii) the period of rapid transition of the EoS parameter from  $w_\phi$  to  $1/3$  (as solid and dashed lines in blue), and (iii) the radiation dominated epoch (in green). We have also demarcated the domain in frequency associated with the thermalization time scales in the figure (as shaded regions in dark and light blue). These quantities have been denoted as  $\Delta f_{\text{th}}^1$  and  $\Delta f_{\text{th}}^3$  for  $w_\phi = 0$  and  $1/2$ , respectively. *Right*: We have illustrated the variation of the frequency  $f_{\text{re}} = k_{\text{re}}/(2\pi)$  as a function of the scalar spectral index  $n_s$  for three different values of  $n = (1, 3, 5)$  (in blue, black and pink) for the  $\alpha$ -attractor model. We have also indicated the 1- $\sigma$  and 2- $\sigma$  confidence regions (as light and dark bands in red) associated with the constraint on scalar spectral index  $n_s$  from Planck [59].

### VIII. CMB, SPECTRUM OF GWS, AND THE MICROSCOPIC REHEATING PARAMETERS

As is well known, the observations of the anisotropies in the CMB by missions such as Planck can be explained in a simple and successful manner by invoking an early phase of inflation [5–14]). Nevertheless, the characterization of the inflaton is far from complete because of the lack of adequate observational constraints, particularly over scales smaller than the CMB scales. The spectrum of GWs is possibly the only probe which can provide us direct access to the physics operating during the epochs of inflation and reheating. In this section, we shall discuss the manner in which we can extract the properties of the inflaton by the combining the observations of the CMB and GWs.

As we have already mentioned, the spectrum of GWs carries signatures which reflect some details of the mechanism of reheating. Recall that, the primary aspect of the reheating phase is the time evolution of the EoS parameter from the initial value of  $w_\phi$  associated with the inflaton to the final value of  $1/3$  corresponding to radiation. The phase can be generically divided into three stages based on the underlying physical processes that operate. In what follows, we shall discuss these stages and the corresponding imprints on  $\Omega_{\text{GW}}(f)$ .

To facilitate the discussion, let us introduce the spectral index  $n_{\text{GW}} = d \ln \Omega_{\text{GW}} / d \ln k$  associated with the spectrum of GWs. Interestingly, we find that all the three stages leave distinct imprints on the spectral index  $n_{\text{GW}}$ , and we have illustrated the behavior of  $n_{\text{GW}}(f)$  for the  $\alpha$ -attractor model (13) in Fig. 6. Note that the first and longest stage is when  $H \ll \Gamma_\phi$ , i.e. when the inflaton is decaying very slowly and hence the background dynamics is dominated by the EoS parameter  $w_\phi$  governing the inflaton. The spectral index  $n_{\text{GW}}$  associated with modes which reenter the Hubble radius during the stage is given by  $n_{\text{GW}} = 2(3w_\phi - 1)/(3w_\phi + 1)$ . In Fig. 6, we have indicated the  $n_{\text{GW}}(f)$  associated with  $w_\phi = 0$  and  $1/2$ . In the subsequent stage, as the Hubble parameter approaches  $\Gamma_\phi$ , the decay of the inflaton becomes increasingly efficient, and the effective EoS parameter begins to change rapidly. The corresponding effects are reflected in the variation of  $n_{\text{GW}}$  over modes which reenter the Hubble radius during the transition, as highlighted in Fig. 6. However, this intermediate stage is the shortest among the three stages and it ends when  $H_{\text{re}} = \Gamma_\phi$ , i.e. when the rate of decay of the inflaton to radiation is at its maximum. The most important of the three stages is the final stage of thermalization which is characterized by the time scale  $\Delta t_{\text{th}}$ . It is the time scale over which the decay products of the inflaton thermalize among themselves. In fact, it is this mechanism that determines the actual initial temperature of the radiation dominated phase contrary to the conventional definition of reheating temperature  $T_{\text{re}}$  defined when  $H = \Gamma_\phi$ . The thermalization process and the associated time scale  $\Delta t_{\text{th}}$  would crucially depend upon nature of all the decay products of the inflaton as well as the detailed dynamics of the decay process. These details will determine the manner in which the EoS parameter changes during this stage and its variation will be imprinted in the behavior of  $n_{\text{GW}}(f)$  as we have illustrated in Fig. 6. Note that there arises a frequency range, say,  $\Delta f_{\text{th}}$ , associated

with the time scale  $\Delta t_{\text{th}}$ , and the variation of the spectral index  $n_{\text{GW}}$  over this domain can provide us with clues to the physics operating during the stage.

Therefore, from the CMB observations and the spectrum of GWs, we can, in principle, extract the following essential information regarding the nature of the inflaton and the underlying physical process taking place during reheating.

(i) *Effective inflaton EoS parameter  $w_\phi$* : The nature of inflaton potential near its minimum or, equivalently, the effective EoS parameter  $w_\phi$  associated with the decay of the inflaton can be determined from the spectral index of GWs through the relation

$$w_\phi = \frac{1}{3} \left( \frac{2 + n_{\text{GW}}}{2 - n_{\text{GW}}} \right). \quad (65)$$

(ii) *Inflaton decay width  $\Gamma_\phi$* : Once we have arrived at the EoS parameter describing the inflaton, the effective inflaton decay constant  $\Gamma_\phi$  can be determined from the CMB and the spectrum of GWs in the following fashion. As we have already mentioned, for modes with wave numbers  $k < k_{\text{re}}$ , the amplitude of the tensor perturbations will remain approximately constant from the time the modes leave the Hubble radius during inflation till they reenter the Hubble radius during the epoch of radiation domination. Due to this reason, over these range of modes, the spectrum of GWs at late times retains the same shape as the spectrum of tensor perturbations generated during inflation. Therefore, using Eq. (56), the scale invariant amplitude of the spectrum of GWs can be utilized to estimate the approximate energy scale near the end of inflation. In the limit of high reheating temperature, we have

$$\Omega_{\text{GW}} h^2 \simeq \Omega_{\text{R}} h^2 \frac{H_1^2}{6 \pi^2 M_{\text{Pl}}^2} \quad (66)$$

and, as a result,

$$H_1 \simeq \left( \frac{6 \pi^2 M_{\text{Pl}}^2 \Omega_{\text{GW}} h^2}{\Omega_{\text{R}} h^2} \right)^{1/2} \quad (67)$$

which, in turn, allows us to express the energy density at the end of inflation as follows:

$$\rho_{\text{f}} \simeq \frac{18 \pi^2 M_{\text{Pl}}^4 \Omega_{\text{GW}} h^2}{\Omega_{\text{R}} h^2}. \quad (68)$$

From the observed spectrum, we can, in principle, determine wave numbers  $k_{\text{re}}$  and  $k_{\text{f}}$ , which are the wave numbers that reenters at the end of the epoch of reheating and leaves the Hubble radius at the end of inflation, respectively. In Fig. 6, we have illustrated the dependence of  $k_{\text{re}}$  on the scalar spectral  $n_{\text{s}}$  for different values of the parameter  $n$  of the  $\alpha$ -attractor model. In a manner similar to the existence of a maximum possible reheating temperature, we notice that there arises a maximum possible value for the frequency associated with the wave number  $k_{\text{re}}$ . We find that, generically,  $f_{\text{re}}^{\text{max}} \simeq 10^7$  Hz, irrespective of the values of the other parameters involved. It would be interesting to study further implications of this point. Nonetheless, the aforementioned wave numbers satisfy the following relations

$$k_{\text{f}} = a_{\text{f}} H_{\text{f}} \simeq a_{\text{f}} H_1, \quad k_{\text{re}} = a_{\text{re}} H_{\text{re}} = A_{\text{re}} a_{\text{f}} \Gamma_\phi. \quad (69)$$

Considering perturbative reheating, one can obtain an approximate analytical expression for the normalized scale factor  $A_{\text{re}}$  at the end of the reheating to be (in this context, see Ref. [93])

$$A_{\text{re}} = \left( \frac{4 \rho_{\text{f}} (1 + w_\phi)^2}{\mathcal{G}^4 \beta (5 - 3 w_\phi)^2} \right)^{-1/(1-3 w_\phi)}, \quad \beta = \frac{\pi^2 g_{\text{r, re}}}{30}, \quad \mathcal{G} = \left( \frac{43}{11 g_{\text{re}}} \right)^{1/3} \left( \frac{a_0 H_1}{k_*} \right) T_0 e^{-N_*}. \quad (70)$$

The primary assumption in arriving at the above expressions is that the energy scale does not change significantly throughout the entire period of inflation. With all the above expressions at hand, we find that the inflaton decay constant  $\Gamma_\phi$  can be written in terms of the observable quantities as

$$\Gamma_\phi = \frac{k_{\text{re}} H_1}{A_{\text{re}} k_{\text{f}}} = \frac{k_{\text{re}}}{k_{\text{f}}} \left( \frac{6 \pi^2 M_{\text{Pl}}^2 \Omega_{\text{GW}} h^2}{\Omega_{\text{R}} h^2} \right)^{1/2} \left( \frac{72 \pi^2 M_{\text{Pl}}^4 \Omega_{\text{GW}} h^2 (1 + w_\phi)^2}{\Omega_{\text{R}} h^2 \mathcal{G}^4 \beta (5 - 3 w_\phi)^2} \right)^{1/(1-3 w_\phi)}. \quad (71)$$

One can then immediately obtain the following analytic expression for the reheating temperature:

$$T_{\text{re}} = \frac{\mathcal{G}}{A_{\text{re}}} = \left( \frac{43}{11 g_{\text{re}}} \right)^{1/3} \frac{k_{\text{f}} H_1}{k_* H_0} \left( \frac{72 \pi^2 M_{\text{Pl}}^4 \Omega_{\text{GW}} h^2 (1 + w_\phi)^2}{\Omega_{\text{R}} h^2 \mathcal{G}^4 \beta (5 - 3 w_\phi)^2} \right)^{1/(1-3 w_\phi)} T_0. \quad (72)$$

So far, we have expressed the inflation decay constant and the reheating temperature in terms of the observables associated with the CMB and the spectrum of GWs today. To understand the exact nature of the coupling, the subsequent thermalization processes right after reheating (i.e. when  $\Gamma_\phi = H_{\text{re}}$ ) becomes important. Therefore, let us now compute the thermalization time scale.

(iii) *Thermalization time scale  $\Delta t_{\text{th}}$* : Thermalization is an important non-equilibrium phenomenon that is ubiquitous in nature. At the end of the phase of reheating, when the rate at which the inflaton decays into radiation has attained a maximum, the subsequent thermalization phase leads to the epoch of radiation domination. In this process, thermalization time scale  $\Delta t_{\text{th}}$  is an important observable which crucially depends on the nature of the initial state as well as the interactions among the internal degrees of freedom. Also, it is the initial state which encodes the information about the coupling between the inflaton and the other fields to which the energy is being transferred. Hence, if we can arrive at  $\Delta t_{\text{th}}$  from the spectrum of GWs, valuable information regarding the fundamental nature of the coupling parameters between the inflation and other fields at very high energies can, in principle, be extracted. The thermalization time scale is defined as

$$\Delta t_{\text{th}} = t_{\text{th}} - t_{\text{re}}, \quad (73)$$

where  $t_{\text{re}}$  is the time corresponding to the end of reheating and  $t_{\text{th}}$  denotes the time at the end of the thermalization process, which leads to the beginning of the actual radiation dominated epoch. In order to obtain an approximate analytic expression, during this regime, we shall assume that the scale factor behaves as  $a \propto t^{2/3(1+w)}$ . This can be justified since we can express the effective EoS parameter during the thermalization phase using the following perturbative expansion:

$$w = \frac{1}{t_{\text{th}} - t_{\text{re}}} \int_{t_{\text{re}}}^{t_{\text{th}}} dt \left[ w_{\text{R}} + (w_\phi - w_{\text{R}}) \frac{\rho_\phi}{\rho_{\text{R}}} + \dots \right] \simeq \frac{1}{3} + \left( w_\phi - \frac{1}{3} \right) x + \mathcal{O}(x^2), \quad x = \frac{1}{t_{\text{th}} - t_{\text{re}}} \int_{t_{\text{re}}}^{t_{\text{th}}} dt \frac{\rho_\phi}{\rho_{\text{R}}}, \quad (74)$$

where  $w_{\text{R}} = 1/3$  is the EoS parameter describing radiation. Note that, during the thermalization phase  $\rho_\phi \ll \rho_{\text{R}}$  and, hence,  $x \ll 1$ . This particular fact enables us to obtain the leading order expression for the thermalization time scale in terms of the observable quantities that we discussed. On utilizing the above form for the EoS parameter, we find that the leading order behavior of the scale factor at  $\Gamma_\phi = H_{\text{re}}$  can be written as

$$a_{\text{re}} \simeq \left( \frac{t_{\text{re}}}{t_1} \right)^{2/[3(1+\omega_{\text{R}})]} \left[ 1 - \frac{2x(w_\phi - w_{\text{R}})}{3(1+w_{\text{R}})^2} \ln \left( \frac{t_{\text{re}}}{t_1} \right) + \dots \right], \quad (75)$$

where  $t_1$  is a constant we have introduced for purposes of normalization. Upon using the relations  $k_{\text{re}} = a_{\text{re}} H_{\text{re}}$ ,  $k_{\text{th}} = a_{\text{th}} H_{\text{th}}$  and  $H_{\text{re}} = \Gamma_\phi$ , we can express the reheating time  $t_{\text{re}}$  and the thermalization time  $t_{\text{th}}$  in terms of the wave numbers  $k_{\text{re}}$  and  $k_{\text{th}}$  as

$$t_{\text{re}} = \left( \frac{k_{\text{th}}}{p_{\text{R}}} \right)^{1/(p_{\text{R}}-1)} t_1^{p_{\text{R}}/(p_{\text{R}}-1)} + \mathcal{O}(x), \quad t_{\text{th}} = \left( \frac{k_{\text{re}}}{p_{\text{R}}} \right)^{1/(p_{\text{R}}-1)} t_1^{p_{\text{R}}/(p_{\text{R}}-1)} + \mathcal{O}(x). \quad (76)$$

We can also express  $\Gamma_\phi$  in terms of normalized time  $t_1$  as

$$\Gamma_\phi \sim \left( \frac{p_{\text{R}}}{t_1} \right)^{p_{\text{R}}/(p_{\text{R}}-1)} k_{\text{re}}^{-1/(p_{\text{R}}-1)} + \mathcal{O}(x), \quad (77)$$

where we have introduced the quantity  $p_{\text{R}} = 2/[3(1+\omega_{\text{R}})]$ . Utilizing all the above equations, we finally obtain the final expression for the thermalization time scale to the leading order in  $x$  to be

$$\Delta t_{\text{th}} \sim \begin{cases} \left[ \left( \frac{k_{\text{th}}}{p_{\text{R}}} \right)^{1/(p_{\text{R}}-1)} - \left( \frac{k_{\text{re}}}{p_{\text{R}}} \right)^{1/(p_{\text{R}}-1)} \right] p_{\text{R}}^{p_{\text{R}}/(p_{\text{R}}-1)} \left( \frac{k_{\text{re}}^{-1/(p_{\text{R}}-1)}}{\Gamma_\phi} \right) + \mathcal{O}(x), & \text{in terms of } \Gamma_\phi, \\ \left[ \left( \frac{k_{\text{th}}}{p_{\text{R}}} \right)^{1/(p_{\text{R}}-1)} - \left( \frac{k_{\text{re}}}{p_{\text{R}}} \right)^{1/(p_{\text{R}}-1)} \right] p_{\text{R}}^{p_{\text{R}}/(p_{\text{R}}-1)} \left( \frac{G k_{\text{re}}^{-p_{\text{R}}/(p_{\text{R}}-1)}}{H_1 T_{\text{re}}} \right) + \mathcal{O}(x), & \text{in terms of } T_{\text{re}}. \end{cases} \quad (78)$$

In the above expressions, an important point one should remember is that the value of the wave numbers  $k_{\text{re}}$  and  $k_{\text{th}}$  are, in general, dependent on the decay width of the inflaton. Therefore, the overall thermalization time scale is a non-trivial function of  $\Gamma_\phi$ .

The thermalization time scale crucially depends on the initial number density of the decayed particles compared with the thermalized ones. The initial number density at the instant when  $\Gamma_\phi = H_{\text{re}}$  can be approximately estimated

to be  $n_i \simeq M_{\text{Pl}}^2 H_{\text{re}}^2 / m_\phi = M_{\text{Pl}}^2 \Gamma_\phi^2 / m_\phi$ , and, in arriving at this expression, it has been assumed that the momentum of the decay products is as large as the mass  $m_\phi$  of the inflaton [125, 126]. If we consider the particles to have thermalized at the reheating temperature  $T_{\text{re}}$ , then the number density can again be approximately determined to be  $n_{\text{th}} \simeq T_{\text{re}}^3 \simeq \Gamma_\phi^{3/2} M_{\text{Pl}}^{3/2}$ . Hence, the ratio of the particle number densities  $n_{\text{th}}$  and  $n_i$  turns out to be

$$\frac{n_{\text{th}}}{n_i} \simeq \frac{m_\phi}{\sqrt{\Gamma_\phi M_{\text{Pl}}}} = \left( \frac{m_\phi^2 A_{\text{re}} k_{\text{f}}}{M_{\text{Pl}} k_{\text{re}} H_{\text{I}}} \right)^{1/2}. \quad (79)$$

This is one of the crucial parameters in the context of the thermalizing plasma which dictates the kind of physical processes that occur during thermalization [125–129]. At this stage, we are unable to extract the inflaton mass  $m_\phi$  from the observations in a model independent manner. However, given the mass of the inflaton, along with the CMB observations, Eq. (79) will have two generic possibilities, viz.

- $n_i < n_{\text{th}}$ : The particle number density is smaller than the thermalized ones, which means that, at the end of reheating, the universe is under occupied. For example if one considers marginal inflaton-scalar ( $\xi$ ) coupling such  $\beta \phi \xi^3$ , inflaton-Fermion ( $\psi$ ) Yukawa coupling  $\beta \phi \bar{\psi} \psi$ , the inflaton decay width behaves as  $\Gamma_\phi \sim \beta^2 m_\phi$  which implies that  $n_i/n_{\text{th}} \sim \sqrt{m_\phi/M_{\text{Pl}}} < 1$ .
- $n_i > n_{\text{th}}$ : The particle number density is larger than the thermalized ones, i.e. at the end of reheating, the universe is over occupied. For example, if one considers any Planck suppressed operator containing a coupling between the inflaton and the reheating field, the decay width behaves as  $\Gamma_\phi \sim m_\phi^3/M_{\text{Pl}}^2$ , which implies that  $n_i/n_{\text{th}} \sim \sqrt{M_{\text{Pl}}}/m_\phi > 1$ .

(iv) *Determination of microscopic interactions*: From our discussion above for the two cases, it is clear that if we can determine the value of  $n_{\text{th}}/n_i$  from the combined observations of the CMB and GWs, the fundamental nature of the inflaton-reheating field coupling such as ‘ $\beta$ ’ can be extracted. Furthermore, interestingly, it has been pointed out that, depending on the aforementioned two conditions for the initial, non-thermal states generated by the end of reheating, the behavior of the thermalization time scale in terms of the microscopic variables will be very different, and will behave as (in this context, see Ref. [125])

$$\Delta t_{\text{th}} \sim \begin{cases} \alpha^{-2} m_\phi^{1/2} T_{\text{th}}^{-3/2}, & \text{for under-occupied initial states such that } n_i < n_{\text{th}}, \\ \alpha^{-2} T_{\text{th}}^{-1}, & \text{for the over-occupied initial state such that } n_i > n_{\text{th}}, \end{cases} \quad (80)$$

where  $\alpha$  denotes the gauge interaction strength among the decayed particles, and  $T_{\text{th}}$  is the final thermalization temperature. Hence, it is extremely important to recognize that, once we know the inflaton mass  $m_\phi$  and the final thermalization temperature  $T_{\text{th}}$  [the latter can be computed once the reheating dynamics is fixed, by using Eqs. (79) and (80)], the gauge interaction strength can, in principle, be computed in terms of the observable quantities through the relations

$$\alpha \sim \begin{cases} T_{\text{th}}^{-1/2} \left[ \left( \frac{k_{\text{th}}}{p_{\text{R}}} \right)^{1/(p_{\text{R}}-1)} - \left( \frac{k_{\text{re}}}{p_{\text{R}}} \right)^{1/(p_{\text{R}}-1)} \right]^{-1/2} p_{\text{R}}^{-p_{\text{R}}/[2(p_{\text{R}}-1)]} \left( \frac{k_{\text{re}}^{-1/(p_{\text{R}}-1)}}{\Gamma_\phi} \right)^{-1/2}, & \text{for } H_{\text{I}} > \frac{m_\phi^2 A_{\text{re}} k_{\text{f}}}{M_{\text{Pl}} k_{\text{re}}}, \\ \left( \frac{m_\phi}{T_{\text{th}}^3} \right)^{1/2} \left[ \left( \frac{k_{\text{th}}}{p_{\text{R}}} \right)^{1/(p_{\text{R}}-1)} - \left( \frac{k_{\text{re}}}{p_{\text{R}}} \right)^{1/(p_{\text{R}}-1)} \right]^{-1/2} p_{\text{R}}^{p_{\text{R}}/[-2(p_{\text{R}}-1)]} \left( \frac{k_{\text{re}}^{-1/(p_{\text{R}}-1)}}{\Gamma_\phi} \right)^{-1/2}, & \text{for } H_{\text{I}} < \frac{m_\phi^2 A_{\text{re}} k_{\text{f}}}{M_{\text{Pl}} k_{\text{re}}}. \end{cases} \quad (81)$$

We expect to carry out a detailed study on these important issues in a future publication. Having examined the effects of the epoch of reheating on the spectrum of GWs today, let us now turn to discuss the effects that arise due to a secondary phase of reheating. As we shall see, such a phase can have an important implication for the recent observational results reported by NANOGrav [94, 95].

## IX. SPECTRUM OF GWS WITH LATE TIME ENTROPY PRODUCTION AND IMPLICATIONS FOR THE RECENT NANOGrAV OBSERVATIONS

In Secs. V and VI, while arriving at the spectrum of GWs  $\Omega_{\text{GW}}(f)$  today, we had assumed that the perturbations were generated during inflation and had evolved through the epochs of reheating and radiation domination. In such a scenario, the entropy of the universe is conserved from the end of reheating until today. In fact, we had earlier



utilized the conservation of entropy to relate the temperature  $T_{\text{re}}$  at the end of reheating to the temperature  $T_0$  today. Recall that, for simplicity, we had assumed that the spectrum of tensor perturbations generated during inflation was strictly scale invariant [cf. Eq. (12)]. We had also found that, for wave numbers  $k < k_{\text{re}}$ , the evolution of the tensor perturbations through the standard epochs of reheating and radiation domination does not alter the shape of the spectrum of GWs observed today, i.e.  $\Omega_{\text{GW}}(f)$  remains scale invariant for  $f < f_{\text{re}} = k_{\text{re}}/(2\pi)$ .

Over the last decade or so, there has been an interest in examining scenarios wherein there arises a short, secondary phase of reheating some time after the original phase of reheating which immediately follows the inflationary epoch (see, for example, Ref. [130]). It has been shown that such a modified scenario can also be consistent with the various observations [71, 131, 132]. A secondary phase of entropy production can occur due to the decay of an additional scalar field (which we shall denote as  $\sigma$ ) that can be present, such as the non-canonical scalar fields often considered in high energy physics or the moduli fields encountered in string theory<sup>1</sup>. In this section, we shall discuss the effects of such a secondary phase of reheating (which occurs apart from the primary phase of reheating considered earlier) on the spectrum of GWs observed today. As we shall see, the secondary phase of entropy production leads to unique imprints on the spectrum of GWs which has interesting implications for the recent observations by NANOGrav [94, 95].

Let us first calculate the reheating temperature associated with the secondary phase of reheating. We can expect the entropy to be conserved during the radiation dominated epoch sandwiched between the two phases of reheating. On following the chronology of evolution mentioned above and, upon demanding the conservation of entropy, we can arrive at the relation between the temperature  $T_{\text{re}}$  at the end of the first phase of reheating and the temperature at the beginning of the second phase of reheating, say,  $T_{\sigma R}$ . We find that they can be related as follows:

$$g_{s,\text{re}} a_{\text{re}}^3 T_{\text{re}}^3 = g_{s,\sigma R} a_{\sigma R}^3 T_{\sigma R}^3, \quad (82)$$

where  $(g_{s,\text{re}}, g_{s,\sigma R})$  and  $(a_{\text{re}}, a_{\sigma R})$  denote the relativistic degrees of contributing to the entropy and the scale factor at the end of primary reheating phase and at the start of the second phase of reheating (or, equivalently, at the end of the first epoch of radiation domination), respectively. Using the above relation, we can express the original reheating temperature  $T_{\text{re}}$  in terms of the temperature  $T_{\sigma R}$  at the beginning of the secondary phase of reheating as

$$T_{\text{re}} = \left( \frac{g_{s,\sigma R}}{g_{s,\text{re}}} \right)^{1/3} e^{N_{\text{RD}}^{(1)}} T_{\sigma R}, \quad (83)$$

where  $N_{\text{RD}}^{(1)} = \ln(a_{\sigma R}/a_{\text{re}})$  denotes the duration of first epoch of radiation domination in terms of the number of e-folds. Similarly, we can relate the temperature at the end of the secondary phase of reheating, say,  $T_{\sigma}$ , to the temperature  $T_0$  today by demanding the conservation of entropy after the onset of the second epoch of radiation domination. On doing so, we obtain that

$$T_{\sigma} = \left( \frac{43}{11 g_{s,\sigma}} \right)^{1/3} \left( \frac{a_0}{a_{\sigma}} \right) T_0, \quad (84)$$

where  $g_{s,\sigma}$  and  $a_{\sigma}$  represent the degrees of freedom contributing to the entropy and the scale factor at the end of the secondary phase of reheating. If  $a_{\text{eq}}$  denotes the scale factor at the epoch of matter-radiation equality, then the above expression for  $T_{\sigma}$  can be written as

$$T_{\sigma} = \left( \frac{43}{11 g_{s,\sigma}} \right)^{1/3} \left( \frac{a_0}{a_{\text{eq}}} \right) e^{N_{\text{RD}}^{(2)}} T_0. \quad (85)$$

The factor  $a_0/a_{\text{eq}}$  can be expressed in terms of the quantity  $a_0/a_k$  through the relation

$$\frac{a_0}{a_{\text{eq}}} = \left( \frac{a_0}{a_k} \right) e^{-[N_k + N_{\text{re}} + N_{\text{RD}}^{(1)} + N_{\text{sre}} + N_{\text{RD}}^{(2)}]}, \quad (86)$$

where  $a_k$  denotes the scale factor when the mode with the wave number  $k$  crosses the Hubble radius during inflation, while  $N_k$  represents the number of e-folds from the time corresponding to  $a_k$  to the end of inflation. Moreover, recall that,  $N_{\text{re}}$  denotes the duration of the first phase of reheating. It should be evident that the quantities  $N_{\text{sre}}$  and  $N_{\text{RD}}^{(2)}$  represent the duration (in terms of e-folds) of the secondary phase of (say, moduli dominated) reheating and the

---

<sup>1</sup> It is for this reason that the secondary phase is sometimes referred to as the moduli dominated epoch. The scalar field could have emerged from an extra-dimensional modulus field or due to some higher curvature effects [133, 134]

second epoch of radiation domination, respectively. With  $k$  set to be the pivot scale  $k_*$ , on substituting the above expression for  $a_0/a_{\text{eq}}$  in Eq. (85), we obtain that

$$T_\sigma = \left( \frac{43}{11 g_{s,\sigma}} \right)^{1/3} \left( \frac{a_0 H_1}{k_*} \right) e^{-[N_* + N_{\text{re}} + N_{\text{RD}}^{(1)} + N_{\text{sre}}]} T_0, \quad (87)$$

which is the temperature at the end of the secondary phase of reheating.

Note that the above expression for  $T_\sigma$  can be inverted to write  $N_{\text{RD}}^{(1)}$  as

$$e^{N_{\text{RD}}^{(1)}} = \left( \frac{43}{11 g_{s,\sigma}} \right)^{1/3} \left( \frac{a_0 H_1}{k_* s t} \right) e^{-[N_* + N_{\text{re}} + N_{\text{sre}}]} \left( \frac{T_0}{T_\sigma} \right). \quad (88)$$

This relation, along with Eq. (83), immediately leads to the following expression for the original reheating temperature  $T_{\text{re}}$  in terms of the parameters associated with the late time entropy production:

$$T_{\text{re}} = \left( \frac{43}{11 g_{s,\text{re}}} \right)^{1/3} \left( \frac{a_0 H_1}{k_*} \right) F^{-1/3} e^{-(N_* + N_{\text{re}})} T_0. \quad (89)$$

In this relation, the factor  $F$  represents the ratio of the entropy at the end and at the beginning of the secondary phase of reheating, and it is given by

$$F = \frac{s(T_\sigma) a_\sigma^3}{s(T_{\sigma R}) a_{\sigma R}^3}, \quad (90)$$

where  $s(T)$  denotes the entropy at the temperature  $T$ . If we now assume that the secondary phase of reheating is described by the EoS parameter  $w_\sigma$ , then we can arrive at the following useful relations between the Hubble parameter and the temperature at the end and at the beginning of the secondary phase of reheating:

$$H_\sigma = \left( \frac{\gamma_1 T_\sigma}{\gamma_2 F^{1/3} T_{\sigma R}} \right)^{3(1+w_\sigma)/2} H_{\sigma R}, \quad T_\sigma = \left( \frac{\gamma_1}{\gamma_2 F^{1/3}} \right)^{3(1+w_\sigma)/(1-3w_\sigma)} \left( \frac{g_{r,\sigma R}}{g_{r,\sigma}} \right)^{1/(1-3w_\sigma)} T_{\sigma R}, \quad (91)$$

where the quantities  $\gamma_1$  and  $\gamma_2$  are defined as

$$\gamma_1 = \left( \frac{g_{r,\text{re}}}{g_{r,\sigma R}} \right)^{1/4}, \quad \gamma_2 = \left( \frac{g_{s,\text{re}}}{g_{s,\sigma}} \right)^{1/3}. \quad (92)$$

Clearly, the factor  $F$  controls the extent of entropy produced at late times. And, in the absence of such entropy production, the factor  $F$  reduces to unity. Also, in such a case, the expression (89) for the reheating temperature  $T_{\text{re}}$  reduces to the earlier expression (33b), as required.

Let us now turn to discuss the spectrum of GWs that arises in such a modified scenario. As we mentioned above, for simplicity, we shall assume that the secondary phase of reheating is described by the EoS parameter  $w_\sigma$ . In order to arrive at  $\Omega_{\text{GW}}(k)$  in the new scenario, we shall follow the calculations described in Sec. V wherein we have evaluated the spectrum analytically. To highlight all the relevant scales involved and also to aid our discussion below, in Fig. 7, we have illustrated the evolution of the comoving Hubble radius in the modified scenario. Specifically, in the figure, we have indicated the new scales  $k_{\sigma R}$  and  $k_\sigma$  which are the wave numbers that reenter the Hubble radius at the start and at the end of the secondary phase of reheating.

Before we go on to illustrate the results, let us try to understand the shape of  $\Omega_{\text{GW}}(k)$  that we can expect in the modified scenario involving late time production of entropy.

- *For wave numbers  $k < k_\sigma$ :* As we mentioned above,  $k_\sigma$  represents the wave number of the mode that reenters the Hubble radius at the onset of the second epoch of radiation domination or, equivalently, at the end of the secondary phase of reheating. Therefore, the range of wave numbers  $k < k_\sigma$  (but with wave numbers larger than those corresponding to the CMB scales) reenter the the Hubble radius during the second epoch of radiation domination. Since they are on super-Hubble scales prior to their reentry, they are not influenced by the background dynamics during the earlier epochs. Hence, the spectrum of GWs for these range of modes can be expected to be scale invariant, which implies that the corresponding spectral index  $n_{\text{GW}}$  vanishes identically.
- *For wave numbers  $k_\sigma < k < k_{\sigma R}$ :* Recall that,  $k_{\sigma R}$  denotes the wave number that reenters the Hubble radius at the beginning of the secondary phase of reheating. As in the case of modes that reenter the primary phase of

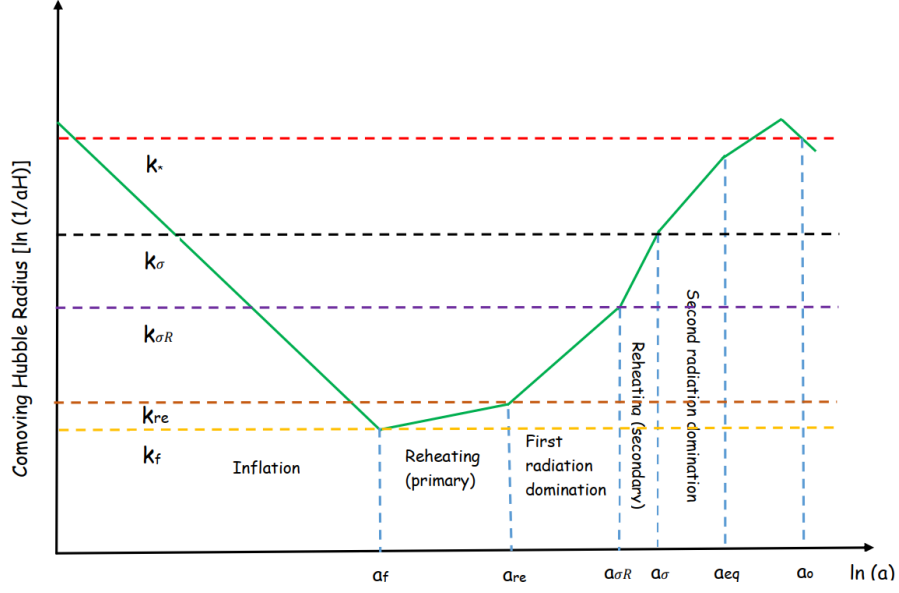


FIG. 7. A schematic diagram illustrating the evolution of the comoving Hubble radius  $(aH)^{-1}$  plotted (in green) against the number of e-folds  $N = \ln a$ . In the diagram, we have also delineated the various epochs that are relevant for our discussion. In the above plot, we have assumed that the EoS parameter  $w_\phi$  describing the primary reheating phase is less than  $1/3$ . However, we have assumed that the EoS parameter, say,  $w_\sigma$ , associated with a string modulus or a non-canonical scalar field driving the secondary phase of reheating is greater than  $1/3$ . In the figure, apart from the wave numbers  $k_*$ ,  $k_{re}$  and  $k_f$  we had encountered earlier (indicated as red, brown and yellow, dashed lines), we have indicated the scales  $k_{\sigma R}$  and  $k_\sigma$  (as dashed lines in purple and black) which correspond to wave numbers that reenter the Hubble radius at the beginning and at the end of the second phase of reheating, respectively.

reheating, we can expect the spectrum of GWs over this range of wave numbers to exhibit a spectral tilt which depends on the EoS parameter  $w_\sigma$ . We find that, over this range of wave numbers,  $\Omega_{\text{GW}}(k)$  behaves as

$$\Omega_{\text{GW}}(k) \sim k^{2(3w_\sigma - 1)/(3w_\sigma + 1)}. \quad (93)$$

Consequently, the spectral index of the primordial GWs over this range of wave numbers turns out to be  $n_{\text{GW}} = 2(3w_\sigma - 1)/(3w_\sigma + 1)$ . In other words, over the domain  $k_\sigma < k < k_{\sigma R}$ , the spectrum has a blue tilt for  $w_\sigma > 1/3$  and a red tilt for  $w_\sigma < 1/3$ .

- *For wave numbers  $k_{\sigma R} < k < k_{re}$ :* These range of wave numbers reenter the Hubble radius during the first epoch of radiation domination. Hence, we can expect the spectrum of GWs to be scale invariant over this range. It is important to recognize that the amplitude of the spectrum  $\Omega_{\text{GW}}(k)$  over this range will be greater or lesser than the amplitude over  $k < k_\sigma$  (i.e. over wave numbers which reenter the Hubble radius during the second epoch of radiation domination) depending on whether the EoS parameter  $w_\sigma$  (characterizing the second phase of reheating) is greater than or less than  $1/3$ .
- *For wave numbers  $k_{re} < k < k_f$ :* These correspond to wave numbers that reenter the Hubble radius during the first phase of reheating and, as we have discussed before, the spectrum of GWs over this range of wave numbers is expected to behave as

$$\Omega_{\text{GW}}(k) \sim k^{2(3w_\phi - 1)/(3w_\phi + 1)}. \quad (94)$$

In other words, the corresponding spectral index is given by  $n_{\text{GW}} = 2(3w_\phi - 1)/(3w_\phi + 1)$ , which has a blue or red tilt depending on whether  $w_\phi$  is greater than or less than  $1/3$ .

The behavior we have highlighted above can be clearly seen in Fig. 8 wherein we have plotted the quantity  $\Omega_{\text{GW}}(f)$  in scenarios involving the second phase of reheating. In arriving at the plots in the figure, we have set the inflaton the EoS parameter to be  $w_\phi = 0$  and have assumed that  $T_{\sigma R} = 1 \text{ GeV}$ . Note that, for a given inflaton EoS parameter  $w_\phi$ , we have two parameters, viz.  $n_s$  and  $F$ , which control the global shape of the spectrum of GWs. We have plotted the

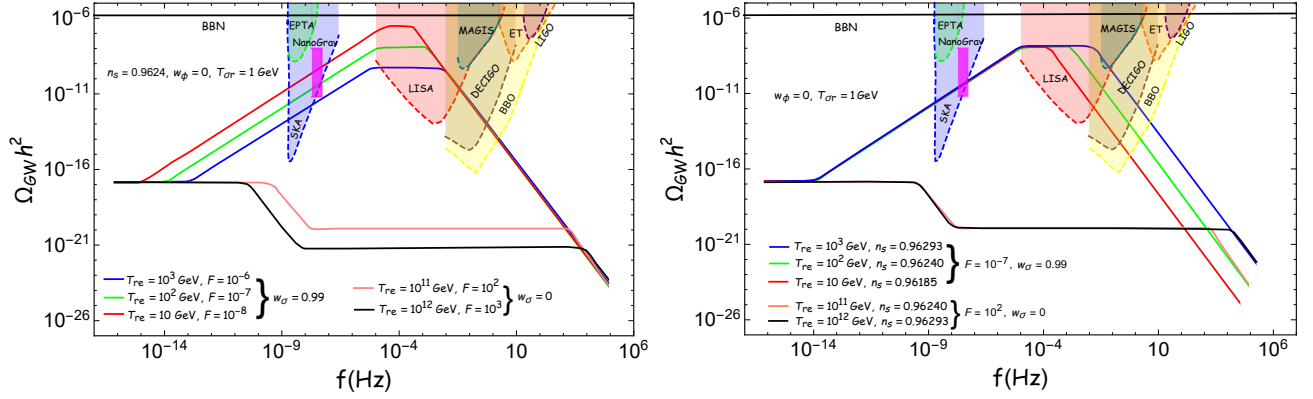


FIG. 8. The spectrum of GWs observed today  $\Omega_{\text{GW}}(f)$  has been plotted in the modified scenario with late time production of entropy. We have illustrated the results for the cases wherein  $n_s$  is fixed and the quantity  $F$  is varied (on the left) as well as for the cases wherein  $F$  is fixed and  $n_s$  is varied (on the right). We have set  $w_\phi = 0$  and  $T_{\sigma R} = 1 \text{ GeV}$  in arriving at the above plots. Also, we have considered the extreme values for  $w_\sigma$  to demonstrate the maximum levels of impact that the generation of entropy at late times can have on the spectrum of GWs. Interestingly, we find that for a set of values of the parameters associated the secondary phase of reheating, the spectrum  $\Omega_{\text{GW}}$  can have amplitudes as suggested by the recent observations by NANOGrav [94, 95].

spectrum for different values of  $F$  with a fixed value of  $n_s$  as well as for different values of  $n_s$  with a fixed  $F$ . In order to highlight the effects due to the additional generation of entropy, we have plotted the results for the limiting values of zero and unity for the EoS parameter  $w_\sigma$  governing the second phase of reheating. We should point that, if a canonical scalar field also dominates the secondary phase of reheating, then for  $V(\sigma) \propto \sigma^{2n}$ , we have  $w_\sigma = (n-1)/(n+1)$  so that for the above mentioned limiting values can be achieved for  $n = 1$  and  $n \rightarrow \infty$ , respectively. One can also consider a more exotic, non-canonical, scalar field with a Lagrangian density of the form  $\mathcal{L} \sim (\partial\sigma)^\mu - \sigma^{2n}$ , where  $\mu$  is a rational number, to drive the second phase of reheating. In such a case, it can be shown that the EoS parameter is given by (in this context, see, for example, Ref. [135])

$$w_\sigma = \frac{n - \mu}{n(2\mu - 1) + \mu}, \quad (95)$$

with the expression reducing to the canonical result for  $\mu = 1$ , as required. Such a model can lead to the extreme values of  $w_\sigma = 0$  (for  $n = \mu$ ) and  $w_\sigma \simeq 1$  for  $[n \simeq \mu/(1 - \mu)]$  that we have considered, without unnaturally large values for a dimensionless number, as it occurs in the canonical case. It seems worthwhile to explore such models in some detail as they could have interesting phenomenological implications.

We find that the effects on  $\Omega_{\text{GW}}(f)$  over the range  $f < f_{\text{re}}$  due to the late time creation of entropy have important implications for the recent observations by the NANOGrav mission. Recall that, recent observations by the NANOGrav mission suggest a stochastic GW background with an amplitude of  $\Omega_{\text{GW}} h^2 \simeq 10^{-11}$  around the frequency of  $10^{-8} \text{ Hz}$  [94, 95]. Clearly, the frequency lies in the domain  $f < f_{\text{re}}$ . In the absence of a second phase of reheating, evidently, the amplitude of  $\Omega_{\text{GW}}$  in the nano-Hertz range of frequencies is rather small, much below the sensitivity of the NANOGrav mission, as we had seen in Secs. V and VI. However, as we have discussed, the late time decay of an additional scalar field such as the moduli field leads to a spectrum with a blue tilt for  $w_\sigma > 1/3$  over the frequency range  $f_\sigma < f < f_{\sigma R}$ , where  $f_\sigma$  and  $f_{\sigma R}$  are the frequencies associated with the wave numbers  $k_\sigma$  and  $k_{\sigma R}$ . Therefore, in such a modified scenario, it is possible to construct situations that result in  $\Omega_{\text{GW}}$  of the strength indicated by NANOGrav, albeit with rather large values for  $w_\sigma$  and relatively low values of the reheating temperature of  $10 < T_{\text{re}} < 10^3 \text{ GeV}$ , as illustrated in Fig. 8. To motivate high values for the EoS parameter, as we mentioned, it seems interesting to consider a non-canonical model of a scalar field that leads to an EoS parameter as in Eq. (95). We should clarify that, to avoid pathological behavior, in the model, we can consider parameters lying within the domains  $n > 0$  and  $\mu > 0$ . In such a case, one can obtain that  $w_\sigma \sim 1$  for  $\mu$  in the range  $0 < \mu < 1$ . Moreover, note that, in the modified scenario with late time entropy production, to be compatible with the NANOGrav results, the reheating temperature  $T_{\text{re}}$  has to be less than  $10^3 \text{ GeV}$ , which implies a low decay width for the inflaton. Further, from Fig. 8, it can be easily seen that the modified scenario can be strongly constrained by many of the forthcoming GW observatories such as SKA, BBO, LISA and DECIGO.

In the pulsar-timing data considered by NANOGrav, the spectrum of the characteristic strain  $h_c(f)$  induced by the

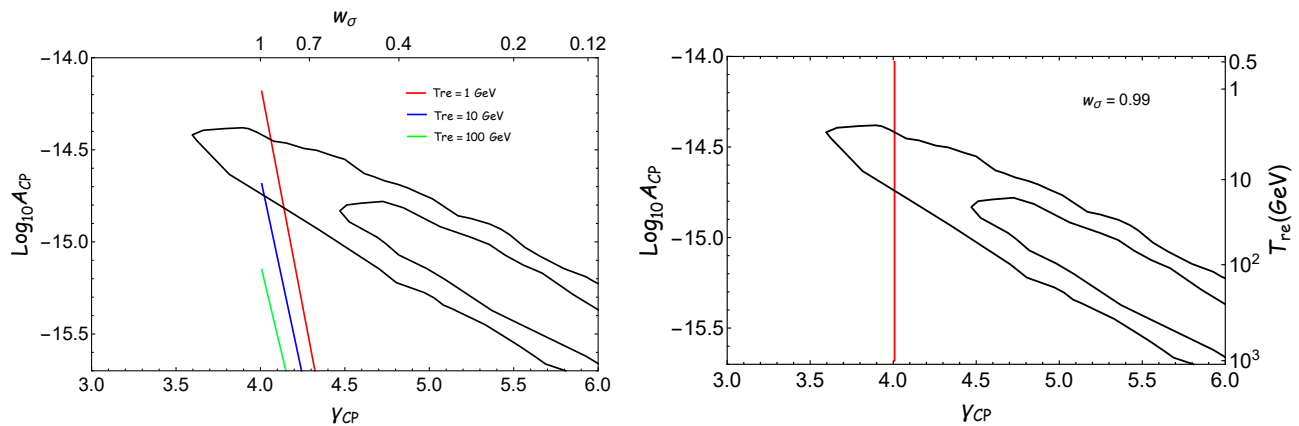


FIG. 9. The constraints from NANOGrav on the parameters  $A_{CP}$  and  $\gamma_{CP}$  have been utilized to illustrate the corresponding constraints on the EoS parameter  $w_\sigma$  describing the secondary phase of reheating and the reheating temperature  $T_{re}$  associated with the primary phase. In the figures, we have included the 1- $\sigma$  and 2- $\sigma$  contours (in black) arrived at by the NANOGrav analysis based on the five-frequency power-law fit [94]. We have projected the results into the  $\gamma_{CP}$ - $A_{CP}$  plane for the following two possibilities: (i) a scenario wherein  $T_{re}$  is fixed and the parameter  $w_\sigma$  is varied (on the left), and (ii) a scenario wherein  $w_\sigma$  is fixed and  $T_{re}$  is varied (on the right). Note that we have assumed that  $w_\phi = 0$  and  $T_{\sigma R} = 0.1$  GeV in arriving at the above plots.

GWs is assumed to be a power law of the form [94, 95]

$$h_c(f) = A_{CP} \left( \frac{f}{f_{yr}} \right)^{(3-\gamma_{CP})/2}, \quad (96)$$

where  $A_{CP}$  refers to the amplitude at the reference frequency  $f_{yr} = 1 \text{ yr}^{-1} = 3.17 \times 10^{-8} \text{ Hz}$ , and  $\gamma_{CP}$  is the timing-residual cross-power spectral density. The dimensionless energy density of GWs today  $\Omega_{GW}(f)$  is related to characteristic strain  $h_c(f)$  induced by the GWs through the relation (in this context, see the recent review [136])

$$\Omega_{GW}(f) = \frac{2\pi^2 f^2}{3H_0^2} h_c^2(f). \quad (97)$$

Upon utilizing the form (96) for the characteristic strain, the energy density of GWs today can be expressed in terms of the amplitude  $A_{CP}$  and the index  $\gamma_{CP}$  as follows:

$$\Omega_{GW}(f) = \frac{2\pi^2 f_{yr}^2}{3H_0^2} A_{CP}^2 \left( \frac{f}{f_{yr}} \right)^{5-\gamma_{CP}}. \quad (98)$$

As we have discussed above, in the scenario with late time entropy production, it is the power associated with the modes that reenter the Hubble radius during the secondary phase of reheating that are consistent with the NANOGrav results [cf. Fig. 8]. Over this domain of wave numbers, since the index of the spectrum of GWs is given by  $n_{GW} = 2(3w_\sigma - 1)/(3w_\sigma + 1)$ , where  $w_\sigma$  is the EoS parameter describing the secondary phase of reheating, clearly, we can set  $\gamma_{CP} = 5 - n_{GW}$ . We can utilize the constraints from the NANOGrav results on the parameters  $A_{CP}$  and  $\gamma_{CP}$  to arrive at the corresponding constraints on, say, the EoS parameter  $w_\sigma$  and the reheating temperature  $T_{re}$  associated with the primary phase. We have illustrated these constraints in Fig. 9. We have illustrated the constraints for the two possibilities, viz. with the reheating temperature  $T_{re}$  associated with the primary phase fixed and the EoS parameter  $w_\sigma$  describing the secondary phase of reheating varied as well as with  $w_\sigma$  fixed and  $T_{re}$  varied. These constraints suggest that only low reheating temperatures (say,  $T_{re} < 10$  GeV) and very high values of the EoS parameter  $w_\sigma$  (with  $w_\sigma \simeq 1$ ) are compatible with the NANOGrav data.

## X. CONCLUSIONS

In this work, we have attempted to understand the effects of reheating on the spectrum of primordial GWs observed today. As a specific example, we had considered the so-called  $\alpha$ -attractor model of inflation and had evolved the tensor

perturbations from the end of inflation through the epochs of reheating and radiation domination to eventually arrive at the spectrum of GWs today. Moreover, we had considered two different scenarios to achieve reheating. In the first scenario, the epoch is described by a constant EoS parameter  $w_\phi$  and the transition to radiation domination is expected to occur instantaneously [87]. Such a simpler modeling of the reheating mechanism had allowed us to study the evolution of the GWs analytically. In the second and more realistic scenario of perturbative reheating wherein the evolution of the energy densities are governed by the Boltzmann equations, the inflaton decays gradually and the transition to the epoch of radiation domination occurs smoothly. The effective EoS parameter in such a scenario changes continuously from its initial value of  $w_{\text{eff}} = w_\phi$  to the final value of  $w_{\text{eff}} = 1/3$ . As it proves to be difficult to obtain analytical solutions in the perturbative reheating scenario, we had examined the problems at hand numerically.

Note that we are interested in the spectrum of GWs today over scales that are considerably smaller than the CMB scales. These scales reenter the Hubble radius either during the phase of reheating or during the epoch of radiation domination. In both the models of reheating we have considered, the spectrum of GWs today  $\Omega_{\text{GW}}(f)$  is scale invariant over wave numbers that reenter the Hubble radius during the epoch of radiation domination (i.e. for  $k < k_{\text{re}}$ ). The scale invariant amplitude over this domain can help us extract the inflationary energy scale in terms of the present radiation abundance since  $H_1^2/M_{\text{Pl}}^2 \sim 6\pi^2 \Omega_{\text{GW}}/\Omega_{\text{R}}$  [cf. Eq. (66)]. The spectrum of GWs today has a tilt over wave numbers  $k_{\text{re}} < k < k_{\text{f}}$  which reenter the Hubble radius during the phase of reheating. The spectral tilt  $n_{\text{GW}} = 2(3w_\phi - 1)/(3w_\phi + 1)$  is red or blue depending on whether  $w_\phi < 1/3$  or  $w_\phi > 1/3$ . Clearly, the observation of the tilt will allow us to determine the reheating parameters such as the EoS parameter  $w_\phi$  and the reheating temperature  $T_{\text{re}}$ . These will allow us to determine the behavior of the inflaton near the minimum of the potential. Moreover, the constraint on the reheating parameters, in turn, can help us constrain the inflationary parameters such as the scalar spectral index  $n_{\text{s}}$ . Further, in the realistic perturbative reheating scenario, there arises an important feature in the spectrum of GWs around wave numbers that reenter the Hubble radius towards the end of the phase of reheating. The spectrum exhibits distinct oscillations near the frequency  $f_{\text{re}}$  and we find that the width of the oscillation reflects the time scale over which the EoS parameter changes from the inflaton dominated value of  $w_\phi$  to that of  $1/3$  in the radiation dominated epoch (cf. Figs. 3 and 4). In fact, the peak of the oscillation occurs at  $f_{\text{re}}$ , which can be associated with the end of perturbative reheating (i.e. when  $H = \Gamma_\phi$ ). We find that, at this instant, the rate of change of the effective EoS parameter exhibits a maximum. This can help us further in determining the inflaton decay rate  $\Gamma_\phi$  in terms of the observed quantities, as expressed in Eq. (71). The end of reheating is to be followed by the most important stage of thermalization. From the width of the oscillation in the spectrum, one can extract information about thermalization time scale  $\Delta t_{\text{th}}$  [cf. Eq. (78)] as well as the nature of the thermalization process depending upon over-occupied or under occupied initial state set by the end of reheating [cf. Eq. (80)]. It turns out that the ratio of the thermalized particle density to the initial decaying particle density (i.e.  $n_{\text{th}}/n_{\text{i}}$ ) depends on the inflaton mass, inflationary energy scale and the wave numbers  $k_{\text{re}}$  and  $k_{\text{f}}$ . Therefore, given the inflaton mass, the spectrum of primordial GWs at the present epoch can be utilized to determine the ratio  $n_{\text{th}}/n_{\text{i}}$ , which is one of the important parameters describing the thermalizing plasma. Once the value of  $n_{\text{th}}/n_{\text{i}}$  is extracted, the strength of the gauge interaction, say,  $\alpha$ , among the reheating decay products can be obtained [cf. Eq. (81)]. We should mention that the oscillatory feature in the spectrum of GWs is encountered for all possible values of  $w_\phi$  and  $T_{\text{re}}$ . We find that the range of frequencies around which the oscillations arise shifts towards higher frequencies as the reheating temperature increases. This can be attributed to the fact that, for a higher value of  $T_{\text{re}}$ , the duration of reheating proves to be shorter and, as a result, the wave number  $k_{\text{re}}$  which reenters at the end of reheating becomes larger.

Apart from the effects due to the standard phase of reheating, we had also considered the signatures on the spectrum of GWs due to a secondary phase of reheating. Such a secondary phase can arise due to the decay of additional scalar fields such as the moduli fields, which can lead to the production of entropy at late times. The moduli dominated phase, which can be described by a constant EoS parameter  $w_\sigma$  (as the primary phase of reheating), leads to a tilt in the spectrum over the range of wave numbers that reenter the Hubble radius during the epoch. Remarkably, we have shown that, for  $w_\sigma > 1/3$  and certain values of the reheating temperature, the production of entropy at late times can lead to  $\Omega_{\text{GW}}(k)$  that correspond to the strengths of the stochastic GW background suggested by the recent NANOGrav observations [94, 95]. We should clarify that such a possibility cannot arise in the conventional reheating scenario wherein the entropy remains conserved from the end of reheating until the present epoch. In fact, the assumption of the secondary phase of reheating and the NANOGrav observations indicate a low reheating temperature of  $T_{\text{re}} \lesssim 10^3$  GeV. We are currently examining different models to understand the wider implications of such interesting possibilities.

## ACKNOWLEDGMENTS

M.R.H would like to thank the Ministry of Human Resource Development, Government of India (GoI), for financial assistance. D.M and L.S wish to acknowledge support from the Science and Engineering Research Board (SERB),



Department of Science and Technology (DST), GoI, through the Core Research Grant CRG/2020/003664. L.S also wishes to acknowledge support from SERB, DST, GoI, through the Core Research Grant No CRG/2018/002200.

- 
- [1] S. Hawking, *Phys. Lett. B* **115**, 295 (1982).
- [2] A. H. Guth and S. Pi, *Phys. Rev. Lett.* **49**, 1110 (1982).
- [3] A. A. Starobinsky, *Phys. Lett. B* **117**, 175 (1982).
- [4] J. M. Bardeen, P. J. Steinhardt, and M. S. Turner, *Phys. Rev. D* **28**, 679 (1983).
- [5] V. F. Mukhanov, H. A. Feldman, and R. H. Brandenberger, *Phys. Rept.* **215**, 203 (1992).
- [6] J. Martin, *Braz. J. Phys.* **34**, 1307 (2004), arXiv:astro-ph/0312492.
- [7] J. Martin, *Lect. Notes Phys.* **669**, 199 (2005), arXiv:hep-th/0406011.
- [8] B. A. Bassett, S. Tsujikawa, and D. Wands, *Rev. Mod. Phys.* **78**, 537 (2006).
- [9] L. Sriramkumar, (2009), arXiv:0904.4584 [astro-ph.CO].
- [10] D. Baumann and H. V. Peiris, *Adv. Sci. Lett.* **2**, 105 (2009), arXiv:0810.3022 [astro-ph].
- [11] D. Baumann, in *Theoretical Advanced Study Institute in Elementary Particle Physics: Physics of the Large and the Small* (2009) arXiv:0907.5424 [hep-th].
- [12] L. Sriramkumar, “On the generation and evolution of perturbations during inflation and reheating,” in *Vignettes in Gravitation and Cosmology*, edited by L. Sriramkumar and T. R. Seshadri (2012).
- [13] A. Linde, in *100e Ecole d’Ete de Physique: Post-Planck Cosmology* (2014) arXiv:1402.0526 [hep-th].
- [14] J. Martin, *Astrophys. Space Sci. Proc.* **45**, 41 (2016), arXiv:1502.05733 [astro-ph.CO].
- [15] L. P. Grishchuk, *Zh. Eksp. Teor. Fiz.* **67**, 825 (1974).
- [16] A. A. Starobinsky, *JETP Lett.* **30**, 682 (1979).
- [17] M. C. Guzzetti, N. Bartolo, M. Liguori, and S. Matarrese, *Riv. Nuovo Cim.* **39**, 399 (2016), arXiv:1605.01615 [astro-ph.CO].
- [18] C. Caprini and D. G. Figueroa, *Class. Quant. Grav.* **35**, 163001 (2018), arXiv:1801.04268 [astro-ph.CO].
- [19] B. Abbott *et al.* (LIGO Scientific, Virgo), *Phys. Rev. Lett.* **116**, 131103 (2016), arXiv:1602.03838 [gr-qc].
- [20] B. Abbott *et al.* (LIGO Scientific, Virgo), *Phys. Rev. D* **93**, 122003 (2016), arXiv:1602.03839 [gr-qc].
- [21] B. Abbott *et al.* (LIGO Scientific, Virgo), *Phys. Rev. Lett.* **116**, 241102 (2016), arXiv:1602.03840 [gr-qc].
- [22] B. P. Abbott *et al.* (LIGO Scientific, Virgo), *Phys. Rev. Lett.* **116**, 061102 (2016), arXiv:1602.03837 [gr-qc].
- [23] B. P. Abbott *et al.* (LIGO Scientific, Virgo), *Phys. Rev. Lett.* **116**, 241103 (2016), arXiv:1606.04855 [gr-qc].
- [24] B. P. Abbott *et al.* (LIGO Scientific, VIRGO), *Phys. Rev. Lett.* **118**, 221101 (2017), [Erratum: *Phys. Rev. Lett.* 121, no.12, 129901 (2018)], arXiv:1706.01812 [gr-qc].
- [25] B. P. Abbott *et al.* (LIGO Scientific, Virgo), *Astrophys. J. Lett.* **851**, L35 (2017), arXiv:1711.05578 [astro-ph.HE].
- [26] B. P. Abbott *et al.* (LIGO Scientific, Virgo), *Phys. Rev. Lett.* **119**, 141101 (2017), arXiv:1709.09660 [gr-qc].
- [27] B. P. Abbott *et al.* (LIGO Scientific, Virgo), *Phys. Rev. Lett.* **119**, 161101 (2017), arXiv:1710.05832 [gr-qc].
- [28] R. Abbott *et al.* (LIGO Scientific, Virgo), *Phys. Rev. D* **102**, 043015 (2020), arXiv:2004.08342 [astro-ph.HE].
- [29] B. P. Abbott *et al.* (LIGO Scientific, Virgo), *Astrophys. J. Lett.* **892**, L3 (2020), arXiv:2001.01761 [astro-ph.HE].
- [30] R. Abbott *et al.* (LIGO Scientific, Virgo), *Astrophys. J.* **896**, L44 (2020), arXiv:2006.12611 [astro-ph.HE].
- [31] B. P. Abbott *et al.* (LIGO Scientific, Virgo), *Phys. Rev. Lett.* **118**, 121101 (2017), [Erratum: *Phys. Rev. Lett.* 119, 029901 (2017)], arXiv:1612.02029 [gr-qc].
- [32] M. Punturo *et al.*, *Class. Quant. Grav.* **27**, 194002 (2010).
- [33] B. Sathyaprakash *et al.*, *Class. Quant. Grav.* **29**, 124013 (2012), [Erratum: *Class. Quant. Grav.* 30, 079501 (2013)], arXiv:1206.0331 [gr-qc].
- [34] J. Crowder and N. J. Cornish, *Phys. Rev.* **D72**, 083005 (2005), arXiv:gr-qc/0506015 [gr-qc].
- [35] V. Corbin and N. J. Cornish, *Class. Quant. Grav.* **23**, 2435 (2006), arXiv:gr-qc/0512039 [gr-qc].
- [36] J. Baker *et al.*, (2019), arXiv:1907.11305 [astro-ph.IM].
- [37] N. Seto, S. Kawamura, and T. Nakamura, *Phys. Rev. Lett.* **87**, 221103 (2001), arXiv:astro-ph/0108011.
- [38] S. Kawamura *et al.*, *Class. Quant. Grav.* **28**, 094011 (2011).
- [39] S. Sato *et al.*, *J. Phys. Conf. Ser.* **840**, 012010 (2017).
- [40] S. Kawamura (DECIGO working group), *PoS KMI2019*, 019 (2019).
- [41] P. Amaro-Seoane *et al.*, *GW Notes* **6**, 4 (2013), arXiv:1201.3621 [astro-ph.CO].
- [42] P. Amaro-Seoane *et al.* (LISA), (2017), arXiv:1702.00786 [astro-ph.IM].
- [43] E. Barausse *et al.*, *Gen. Rel. Grav.* **52**, 81 (2020), arXiv:2001.09793 [gr-qc].
- [44] G. Janssen *et al.*, *PoS AASKA14*, 037 (2015), arXiv:1501.00127 [astro-ph.IM].
- [45] R. Easther and E. A. Lim, *JCAP* **04**, 010 (2006), arXiv:astro-ph/0601617.
- [46] K. N. Ananda, C. Clarkson, and D. Wands, *Phys. Rev.* **D75**, 123518 (2007), arXiv:gr-qc/0612013 [gr-qc].
- [47] D. Baumann, P. J. Steinhardt, K. Takahashi, and K. Ichiki, *Phys. Rev.* **D76**, 084019 (2007), arXiv:hep-th/0703290 [hep-th].
- [48] R. Saito and J. Yokoyama, *Phys. Rev. Lett.* **102**, 161101 (2009), [Erratum: *Phys. Rev. Lett.* 107, 069901 (2011)], arXiv:0812.4339 [astro-ph].

- [49] R. Saito and J. Yokoyama, *Prog. Theor. Phys.* **123**, 867 (2010), [Erratum: *Prog.Theor.Phys.* 126, 351–352 (2011)], [arXiv:0912.5317 \[astro-ph.CO\]](#).
- [50] S. Kuroyanagi, T. Chiba, and T. Takahashi, *JCAP* **11**, 038 (2018), [arXiv:1807.00786 \[astro-ph.CO\]](#).
- [51] J. R. Espinosa, D. Racco, and A. Riotto, *JCAP* **09**, 012 (2018), [arXiv:1804.07732 \[hep-ph\]](#).
- [52] K. Kohri and T. Terada, *Phys. Rev. D* **97**, 123532 (2018), [arXiv:1804.08577 \[gr-qc\]](#).
- [53] K. Inomata, K. Kohri, T. Nakama, and T. Terada, *JCAP* **10**, 071 (2019), [arXiv:1904.12878 \[astro-ph.CO\]](#).
- [54] K. Inomata, K. Kohri, T. Nakama, and T. Terada, *Phys. Rev. D* **100**, 043532 (2019), [arXiv:1904.12879 \[astro-ph.CO\]](#).
- [55] M. Braglia, D. K. Hazra, F. Finelli, G. F. Smoot, L. Sriramkumar, and A. A. Starobinsky, *JCAP* **08**, 001 (2020), [arXiv:2005.02895 \[astro-ph.CO\]](#).
- [56] H. V. Ragavendra, P. Saha, L. Sriramkumar, and J. Silk, *Phys. Rev. D* **103**, 083510 (2021), [arXiv:2008.12202 \[astro-ph.CO\]](#).
- [57] H. V. Ragavendra, L. Sriramkumar, and J. Silk, *JCAP* **05**, 010 (2021), [arXiv:2011.09938 \[astro-ph.CO\]](#).
- [58] S. Bhattacharya, S. Mohanty, and P. Parashari, (2020), [arXiv:2010.05071 \[astro-ph.CO\]](#).
- [59] Y. Akrami *et al.* (Planck), *Astron. Astrophys.* **641**, A10 (2020), [arXiv:1807.06211 \[astro-ph.CO\]](#).
- [60] E. Aubourg *et al.*, *Phys. Rev. D* **92**, 123516 (2015), [arXiv:1411.1074 \[astro-ph.CO\]](#).
- [61] J. A. Vázquez, L. E. Padilla, and T. Matos, (2018), 10.31349/RevMexFisE.17.73, [arXiv:1810.09934 \[astro-ph.CO\]](#).
- [62] M. S. Turner, M. J. White, and J. E. Lidsey, *Phys. Rev. D* **48**, 4613 (1993), [arXiv:astro-ph/9306029](#).
- [63] L. A. Boyle and P. J. Steinhardt, *Phys. Rev. D* **77**, 063504 (2008), [arXiv:astro-ph/0512014](#).
- [64] P. M. Sa and A. B. Henriques, *Phys. Rev. D* **77**, 064002 (2008), [arXiv:0712.2697 \[astro-ph\]](#).
- [65] K. Nakayama, S. Saito, Y. Suwa, and J. Yokoyama, *JCAP* **06**, 020 (2008), [arXiv:0804.1827 \[astro-ph\]](#).
- [66] K. Nakayama, S. Saito, Y. Suwa, and J. Yokoyama, *Phys. Rev. D* **77**, 124001 (2008), [arXiv:0802.2452 \[hep-ph\]](#).
- [67] P. M. Sa and A. B. Henriques, *Phys. Rev. D* **81**, 124043 (2010), [arXiv:1003.4112 \[gr-qc\]](#).
- [68] S. Kuroyanagi, K. Nakayama, and S. Saito, *Phys. Rev. D* **84**, 123513 (2011), [arXiv:1110.4169 \[astro-ph.CO\]](#).
- [69] S. Kuroyanagi, T. Takahashi, and S. Yokoyama, *JCAP* **02**, 003 (2015), [arXiv:1407.4785 \[astro-ph.CO\]](#).
- [70] H. Assadullahi and D. Wands, *Phys. Rev. D* **79**, 083511 (2009), [arXiv:0901.0989 \[astro-ph.CO\]](#).
- [71] K. Nakayama and J. Yokoyama, *JCAP* **01**, 010 (2010), [arXiv:0910.0715 \[astro-ph.CO\]](#).
- [72] R. Durrer and J. Hasenkamp, *Phys. Rev. D* **84**, 064027 (2011), [arXiv:1105.5283 \[gr-qc\]](#).
- [73] L. Alabidi, K. Kohri, M. Sasaki, and Y. Sendouda, *JCAP* **05**, 033 (2013), [arXiv:1303.4519 \[astro-ph.CO\]](#).
- [74] F. D’Eramo and K. Schmitz, *Phys. Rev. Research* **1**, 013010 (2019), [arXiv:1904.07870 \[hep-ph\]](#).
- [75] A. Ricciardone and G. Tasinato, *Phys. Rev. D* **96**, 023508 (2017), [arXiv:1611.04516 \[astro-ph.CO\]](#).
- [76] S. Koh, B.-H. Lee, and G. Tumurtushaa, *Phys. Rev. D* **98**, 103511 (2018), [arXiv:1807.04424 \[astro-ph.CO\]](#).
- [77] T. Fujita, S. Kuroyanagi, S. Mizuno, and S. Mukohyama, *Phys. Lett. B* **789**, 215 (2019), [arXiv:1808.02381 \[gr-qc\]](#).
- [78] N. Bernal and F. Hajkarim, *Phys. Rev. D* **100**, 063502 (2019), [arXiv:1905.10410 \[astro-ph.CO\]](#).
- [79] N. Bernal, A. Ghoshal, F. Hajkarim, and G. Lambiase, *JCAP* **11**, 051 (2020), [arXiv:2008.04959 \[gr-qc\]](#).
- [80] S. S. Mishra, V. Sahni, and A. A. Starobinsky, (2021), [arXiv:2101.00271 \[gr-qc\]](#).
- [81] S. Weinberg, *Phys. Rev. D* **69**, 023503 (2004), [arXiv:astro-ph/0306304](#).
- [82] A. Mangilli, N. Bartolo, S. Matarrese, and A. Riotto, *Phys. Rev. D* **78**, 083517 (2008), [arXiv:0805.3234 \[astro-ph\]](#).
- [83] Y. Watanabe and E. Komatsu, *Phys. Rev. D* **73**, 123515 (2006), [arXiv:astro-ph/0604176](#).
- [84] S. Kuroyanagi, T. Chiba, and N. Sugiyama, *Phys. Rev. D* **79**, 103501 (2009), [arXiv:0804.3249 \[astro-ph\]](#).
- [85] R. R. Caldwell, F. L. Smith, and D. G. E. Walker, *Phys. Rev. D* **100**, 043513 (2019), [arXiv:1812.07577 \[astro-ph.CO\]](#).
- [86] J. Martin and C. Ringeval, *Phys. Rev. D* **82**, 023511 (2010), [arXiv:1004.5525 \[astro-ph.CO\]](#).
- [87] L. Dai, M. Kamionkowski, and J. Wang, *Phys. Rev. Lett.* **113**, 041302 (2014), [arXiv:1404.6704 \[astro-ph.CO\]](#).
- [88] J. L. Cook, E. Dimastrogiovanni, D. A. Easson, and L. M. Krauss, *JCAP* **04**, 047 (2015), [arXiv:1502.04673 \[astro-ph.CO\]](#).
- [89] D. J. H. Chung, E. W. Kolb, and A. Riotto, *Phys. Rev. D* **60**, 063504 (1999), [arXiv:hep-ph/9809453](#).
- [90] G. F. Giudice, E. W. Kolb, and A. Riotto, *Phys. Rev. D* **64**, 023508 (2001), [arXiv:hep-ph/0005123](#).
- [91] D. Maity and P. Saha, *Phys. Rev. D* **98**, 103525 (2018), [arXiv:1801.03059 \[hep-ph\]](#).
- [92] M. R. Haque and D. Maity, *Phys. Rev. D* **99**, 103534 (2019), [arXiv:1902.09491 \[hep-th\]](#).
- [93] M. R. Haque, D. Maity, and P. Saha, *Phys. Rev. D* **102**, 083534 (2020), [arXiv:2009.02794 \[hep-th\]](#).
- [94] Z. Arzoumanian *et al.* (NANOGrav), *Astrophys. J. Lett.* **905**, L34 (2020), [arXiv:2009.04496 \[astro-ph.HE\]](#).
- [95] N. S. Pol *et al.* (NANOGrav), (2020), [arXiv:2010.11950 \[astro-ph.HE\]](#).
- [96] S. Kuroyanagi, T. Takahashi, and S. Yokoyama, *JCAP* **01**, 071 (2021), [arXiv:2011.03323 \[astro-ph.CO\]](#).
- [97] K. Inomata, M. Kawasaki, K. Mukaida, and T. T. Yanagida, (2020), [arXiv:2011.01270 \[astro-ph.CO\]](#).
- [98] H. W. H. Tahara and T. Kobayashi, *Phys. Rev. D* **102**, 123533 (2020), [arXiv:2011.01605 \[gr-qc\]](#).
- [99] N. Kitajima, J. Soda, and Y. Urakawa, (2020), [arXiv:2010.10990 \[astro-ph.CO\]](#).
- [100] G. Domènech and S. Pi, (2020), [arXiv:2010.03976 \[astro-ph.CO\]](#).
- [101] H.-H. Li, G. Ye, and Y.-S. Piao, *Phys. Lett. B* **816**, 136211 (2021), [arXiv:2009.14663 \[astro-ph.CO\]](#).
- [102] L. Bian, R.-G. Cai, J. Liu, X.-Y. Yang, and R. Zhou, *Phys. Rev. D* **103**, L081301 (2021), [arXiv:2009.13893 \[astro-ph.CO\]](#).
- [103] S. Blasi, V. Brdar, and K. Schmitz, *Phys. Rev. Lett.* **126**, 041305 (2021), [arXiv:2009.06607 \[astro-ph.CO\]](#).
- [104] V. De Luca, G. Franciolini, and A. Riotto, *Phys. Rev. Lett.* **126**, 041303 (2021), [arXiv:2009.08268 \[astro-ph.CO\]](#).
- [105] V. Vaskonen and H. Veermäe, *Phys. Rev. Lett.* **126**, 051303 (2021), [arXiv:2009.07832 \[astro-ph.CO\]](#).
- [106] J. Ellis and M. Lewicki, *Phys. Rev. Lett.* **126**, 041304 (2021), [arXiv:2009.06555 \[astro-ph.CO\]](#).
- [107] W. Buchmuller, V. Domcke, and K. Schmitz, *Phys. Lett. B* **811**, 135914 (2020), [arXiv:2009.10649 \[astro-ph.CO\]](#).
- [108] K. Kohri and T. Terada, *Phys. Lett. B* **813**, 136040 (2021), [arXiv:2009.11853 \[astro-ph.CO\]](#).
- [109] S. Vagnozzi, *Mon. Not. Roy. Astron. Soc.* **502**, L11 (2021), [arXiv:2009.13432 \[astro-ph.CO\]](#).

- [110] M. Maggiore, *Phys. Rept.* **331**, 283 (2000), arXiv:gr-qc/9909001.
- [111] R. Kallosh and A. Linde, *JCAP* **07**, 002 (2013), arXiv:1306.5220 [hep-th].
- [112] R. Kallosh, A. Linde, and D. Roest, *JHEP* **11**, 198 (2013), arXiv:1311.0472 [hep-th].
- [113] A. A. Starobinsky, *Phys. Lett. B* **91**, 99 (1980).
- [114] F. L. Bezrukov and M. Shaposhnikov, *Phys. Lett. B* **659**, 703 (2008), arXiv:0710.3755 [hep-th].
- [115] M. Drewes, J. U. Kang, and U. R. Mun, *JHEP* **11**, 072 (2017), arXiv:1708.01197 [astro-ph.CO].
- [116] D. I. Podolsky, G. N. Felder, L. Kofman, and M. Peloso, *Phys. Rev. D* **73**, 023501 (2006), arXiv:hep-ph/0507096.
- [117] D. G. Figueroa and F. Torrenti, *JCAP* **02**, 001 (2017), arXiv:1609.05197 [astro-ph.CO].
- [118] D. Maity and P. Saha, *JCAP* **07**, 018 (2019), arXiv:1811.11173 [astro-ph.CO].
- [119] V. Mukhanov, *Physical Foundations of Cosmology* (Cambridge University Press, Oxford, 2005).
- [120] M. R. Haque, D. Maity, and S. Pal, *Phys. Rev. D* **103**, 103540 (2021), arXiv:2012.10859 [hep-th].
- [121] I. S. Gradshteyn and I. M. Ryzhik, *Table of integrals, series, and products*, seventh ed. (Elsevier/Academic Press, Amsterdam, 2007) pp. xlviii+1171, translated from the Russian, Translation edited and with a preface by Alan Jeffrey and Daniel Zwillinger, With one CD-ROM (Windows, Macintosh and UNIX).
- [122] C. Moore, R. Cole, and C. Berry, *Class. Quant. Grav.* **32**, 015014 (2015), arXiv:1408.0740 [gr-qc].
- [123] L. Pagano, L. Salvati, and A. Melchiorri, *Phys. Lett. B* **760**, 823 (2016), arXiv:1508.02393 [astro-ph.CO].
- [124] D. K. Hazra, L. Sriramkumar, and J. Martin, *JCAP* **05**, 026 (2013), arXiv:1201.0926 [astro-ph.CO].
- [125] A. Kurkela and G. D. Moore, *JHEP* **12**, 044 (2011), arXiv:1107.5050 [hep-ph].
- [126] K. Harigaya and K. Mukaida, *JHEP* **05**, 006 (2014), arXiv:1312.3097 [hep-ph].
- [127] J. R. Ellis, K. Enqvist, D. V. Nanopoulos, and K. A. Olive, *Phys. Lett. B* **191**, 343 (1987).
- [128] J. McDonald, *Phys. Rev. D* **61**, 083513 (2000), arXiv:hep-ph/9909467.
- [129] R. Allahverdi, *Phys. Rev. D* **62**, 063509 (2000), arXiv:hep-ph/0004035.
- [130] M. Kawasaki and F. Takahashi, *Phys. Lett. B* **618**, 1 (2005), arXiv:hep-ph/0410158.
- [131] S. Kuroyanagi, C. Ringeval, and T. Takahashi, *Phys. Rev. D* **87**, 083502 (2013), arXiv:1301.1778 [astro-ph.CO].
- [132] H. Hattori, T. Kobayashi, N. Omoto, and O. Seto, *Phys. Rev. D* **92**, 103518 (2015), arXiv:1510.03595 [hep-ph].
- [133] N. Banerjee and T. Paul, *Eur. Phys. J. C* **77**, 672 (2017), arXiv:1706.05964 [hep-th].
- [134] E. Elizalde, S. D. Odintsov, T. Paul, and D. Sáez-Chillón Gómez, *Phys. Rev. D* **99**, 063506 (2019), arXiv:1811.02960 [gr-qc].
- [135] S. Unnikrishnan, V. Sahni, and A. Toporensky, *JCAP* **08**, 018 (2012), arXiv:1205.0786 [astro-ph.CO].
- [136] J. Yokoyama, (2021), arXiv:2105.07629 [gr-qc].